HHS Public Access

Author manuscript

J Comp Neurol. Author manuscript; available in PMC 2017 August 16.

Published in final edited form as:

J Comp Neurol. 2017 March 01; 525(4): 818–849. doi:10.1002/cne.24100.

Cellular Distribution of Fragile X Mental Retardation Protein in the Mouse Brain

Diego A. R. Zorio[1], **Christine M. Jackson**[1], **Yong Liu**[1], **Edwin W Rubel**[2], and **Yuan Wang**[1,*]

[1]Department of Biomedical Sciences, College of Medicine, Florida State University, Tallahassee, FL 32306, USA

[2]Virginia Merrill Bloedel Hearing Research Center, Department of Otolaryngology-Head and Neck Surgery, University of Washington School of Medicine, Box 357923, Seattle, WA 98195, USA

Abstract

The fragile X mental retardation protein (FMRP) plays an important role in normal brain development. Absence of FMRP, caused by transcriptional silencing of FMR1 gene, results in abnormal neuronal morphologies in a selected manner throughout the brain and leads to intellectual deficits and sensory dysfunction in the fragile X syndrome (FXS). Despite the paramount importance of FMRP for proper brain function, its overall expression pattern in the mammalian brain at the resolution of individual neuronal cell groups is not known. In this study, we used FMR1 knockout and their isogenic wild type mice to systematically map the distribution of FMRP expression in the entire mouse brain. Using immunocytochemistry and cellular quantification analyses, we identified a large number of prominent cell groups expressing high levels of FMRP at the subcortical levels, in particular sensory and motor neurons in the brainstem and thalamus. In contrast, many cell groups in the midbrain and hypothalamus exhibit low FMRP levels. More importantly, we describe differential patterns of FMRP distribution in both cortical and subcortical brain regions. Almost all major brain areas contain high and low levels of FMRP cell groups adjacent to each other or between layers of the same cortical areas. These differential patterns indicate that FMRP expression is specific to individual neuronal cell groups, instead of associated with brain regions as previously considered. Taken together, these findings support the notion that FMRP mechanisms of neuronal regulation are cell-type specific and strongly implicate the contribution of fundamental sensory and motor processing at subcortical levels to FXS pathology.

Correspondence to: Yuan Wang, Department of Biomedical Sciences, Florida State University, 1115 West Call Street, Tallahassee, FL 32306, Phone: (850) 645-4934, yuan.wang@med.fsu.edu.

CONFLICT OF INTEREST

The authors have no identified conflict of interest.

DATA ACCESSIBILITY

Upon acceptance of the manuscript, the complete series of high-resolution images of FMRP (7G1) immunostaining will be deposited onto the Biolucida Cloud server maintained by MBF Biosciences.

ROLE OF AUTHORS

All authors had full access to all the data in the study and take responsibility for the integrity of the data and the accuracy of the data analysis. Study concept and design: Wang Y and Rubel EW Acquisition and analysis of data: Wang Y, Jackson C, Yong L, Zorio D. Drafting of the manuscript: Zorio D, Wang Y. Obtained funding: Wang Y.

Keywords

fragile X syndrome; whole brain analyses; cell-type specificity; sensory information processing

Introduction

Loss of the fragile X mental retardation protein (FMRP) leads to fragile X syndrome (FXS) in children, the leading known genetic cause of autism spectrum disorders (Verkerk et al., 1991; Penagarikano et al., 2007; Bagni et al., 2012; Santoro et al., 2012). FMRP is encoded by the X-linked gene FMR1. Transcriptional silencing of FMR1 leads to loss of FMRP protein and abnormal neuronal structure and function (Rudelli et al., 1985; Hinton et al., 1991; Braun and Segal, 2000; Irwin et al., 2001, 2002; Galvez et al., 2003, 2005; McKinney et al., 2005; Levenga et al., 2011; Till et al., 2012). Phenotypically, patients exhibit intellectual disability including learning and memory deficits, communication and social difficulties, as well as sensory and motor dysfunction. Consistent with these observations, FMRP is highly expressed in healthy brains, in particular neuronal structures (Devys et al., 1993; Hinds et al., 1993; Gholizadeh et al., 2015).

To explore FMRP mechanisms in normal brain development and function, as well as the contribution of FMRP loss to FXS phenotypes, it is fundamentally important to understand the expression patterns of FMRP in the brain. Earlier studies reported intensive FMRP expression in the hippocampus, cerebellum, nucleus basalis, cerebral cortex, and olfactory bulb, while detected minimal or generally low levels of FMRP in other brain areas such as corpus callosum, brainstem, and thalamus (Hinds et al., 1993; Devys et al., 1993; Abitbol et al 1993; Bakker et al., 2000; Zangenehpour et al., 2009). More recent studies, however, demonstrated that FMRP is distributed throughout the brain and is expressed in most, if not all, neurons (Feng et al., 1997; Christie et al., 2009). In certain cases, the expression level of FMRP appears highly heterogeneous as shown by Hinds et al. (1993), in which a “dense yet patchy” labeling pattern of FMR1 hybridization in the mouse cortex was observed. In the visual thalamus, high FMRP expression level is detected in the magnocellular, but not parvocellular, neurons of the primate lateral geniculate nucleus (Kogan et al., 2004a). Importantly, this difference is consistent with a selective visual deficit of the magnocellular pathway in FXS individuals (Kogan et al., 2004a, 2004b). In the brainstem, our recent studies have identified high levels of FMRP in auditory neurons as compared to other neuronal cell types in adjacent areas (Beebe et al., 2014; Wang et al., 2014), which is consistent with the reports in FMR1 knockout mice showing reduced cell size, altered synaptic connectivity, and reduced dynamics in ion channel regulation of auditory brainstem neurons (Strumbos et al., 2010; Rotschafer et al., 2015). In addition, FMR1 knockout induced dendritic spine abnormalities is regional-specific in the hippocampus CA1, but not CA3 (Levenga et al., 2011). These studies emphasize the importance of identifying FMRP-rich neuronal cell types in normal brains, as they could potentially be the prominent targets of FMRP loss and thus reasonable candidates for exploring FXS pathology.

Although a systematic map of a specialized presynaptic format of FMRP has been previously reported (Christie et al., 2009; Akins et al., 2012), the overall FMRP distribution

in the entire mammalian brain at the resolution of individual neuronal cell groups is not known. Therefore there is still a critical need to establish the pattern of FMRP expression throughout the different types of neuronal cells to further increase our knowledge on FMRP function in the brain. Using immunocytochemistry, the current study provides a detailed analysis of FMRP distribution in the whole brain of FVB mice, as the FMR1 knockout strain on this genetic background is commonly used for studying FMRP loss-induced neuronal deficits and for testing drug candidates for rescuing FXS phenotypes (for example, Bakker et al., 1994; Fisch et al., 1999; Chen and Toth, 2001; Irwin et al., 2002; Strumbos et al., 2010; La Fata et al., 2014). As compared to their isogenic wild type mice, FMR1 knockout mice on FVB background exhibit volume changes in more brain regions than FMR1 knockout mice on C57BL/6 background (Lai et al., 2016) and they show more dramatic behavioral alterations (Pietropaolo et al., 2011).

The data presented in this study demonstrate for the first time the identification of a number of distinct neuronal cell types that are particularly rich in FMRP at the subcortical levels, as well as differential patterns of FMRP distribution in both the cortical and subcortical brain regions.

MATERIALS AND METHODS

Animals

FMR1 knockout (Hemi FVB.129P2-Pde6b+; #004624) mice and their wild-type littermates (FVB.129P2-Pde6b+; #004828) were purchased from the Jackson Laboratory (Bar Harbor, ME). Six (6) wild-type and four (4) knockout animals of 5–6 weeks old were used in this study. All procedures were approved by the Florida State University Institutional Animal Care and Use Committee and conformed to NIH guidelines.

Immunocytochemistry

The animals were anesthetized with a mixture of 100 mg/kg ketamine and 15 mg/kg xylazine and transcardially perfused with 0.9% saline followed by 4% paraformaldehyde in 0.1 M phosphate buffer (PB). The brains were removed from the skull, post-fixed overnight in the same fixative. The brains were then transferred to 30% sucrose in PB until they sank and cut either coronally (3 wild-type and 2 knockout) or parasagittally (3 wild-type and 2 knockout) at 30 μm on a freezing sliding microtome. Sections were collected in 0.01 M phosphate buffered saline (PBS) into four alternate sets of serial sections and stained for Nissl substance or immunocytochemistry.

For peroxidase immunostaining for FMRP, the sections were mounted on gelatin-coated slides and dried at 37°C overnight. Sections were then washed in PBS for 15 minutes, pretreated with 0.1% sodium borohydride in PBS for 10 minutes, washed in PBS for 15 minutes, incubated in heated 10 mM citrate buffer (pH 6.0) for 20 minutes, washed in PBS for 10 minutes, followed by 50 mM ammonium chloride in PBS for 15 minutes, then finally washed in PBS for 10 minutes. After treatment, sections were incubated with primary antibody solutions diluted 1:500 in PBS with 0.3% Triton X-100 overnight at 4°C, followed by biotinylated goat anti-IgG antibodies (1:200; Vector Laboratories, Burlingame, CA) for

one hour at room temperature. Sections were incubated in avidin-biotin-peroxidase complex solution (ABC Elite kit; Vector Laboratories) diluted 1:100 in PBS with 0.3% Triton X-100 for 1 hour at room temperature. For visualization, sections were incubated for 3–7 minutes in 0.015% 3-3′-diaminobenzidine (Sigma, St. Louis, MO), either with 0.01% hydrogen peroxide in PBS or with 0.03% hydrogen peroxide, 125 mM sodium acetate, 10 mM imidazole, and 100 mM nickel ammonium sulfate. Sections were then dehydrated, cleared, and coverslipped with DPX mounting medium (EMS, Hatfield, PA).

Antibody characterization

A number of monoclonal and polyclonal antibodies have been produced to detect FMRP. All of these antibodies detect FMRP bands on Western blot. However, many of them are not specific as evidenced by extra bands on Western blot in addition to FMRP (data not shown). While these antibodies provide a useful tool for Western blot and immunoprecipitation studies which separate FMRP from other proteins of different molecular weights or structure, it is challenging for studying cellular and subcellular protein localization in intact tissue samples using immunocytochemistry. Out of 13 commercially available anti-FMRP antibodies tested in our lab, we chose two antibodies, the 7G1 and 2F5, to use for immunocytochemistry, as they show the most specific detection of the mouse FMRP in both Western blot and immunocytochemistry.

Monoclonal anti-FMRP antibody 7G1 was first generated by Brown et al. (2001) by immunizing FMR1 knockout mice with hexahistidine-tagged FMRP. The FMRP-epitope recognized by 7G1 is amino acid 354-368 of the mouse FMRP, in a region with no homology to the fragile X-related paralogs. The specificity of the antibody was characterized by Western blot in Brown et al. (2001) and further tested by both Western blot and immunocytochemistry in the current study (see the Results).

Monoclonal anti-FMRP antibody 2F5 was produced by Gabel et al. (2004) by immunizing FMR1 knockout mice with an N-terminal fragment of human FMRP (residues 1-204). Immunocytochemical and Western blot analysis of wild-type and FMR1 knockout mice demonstrate that 2F5 is specific for FMRP, as first characterized in Gabel et al. (2004) and confirmed in the current study (see the Results). The 2F5 antibody used in the current study was initially provided generously by Dr. Jennifer Darnel at the Rockefeller University and then purchased from the Developmental Studies Hybridoma Bank (DSHB).

It is worthy to note that neither 7G1 nor 2F5 reveal substantial dendritic staining by light microscopy, except of the most proximal part of dendrites in some, but not all, neurons. Our previous study with a polyclonal antibody ab17722 (Abcam; San Faranscisco, CA) (Wang et al., 2014) reveals prominent FMRP clusters throughout dendritic branches in the brainstem. Unfortunately, the subsequent batches of the antibody lost specificity when compared to the previous batch, exhibiting non-FMRP staining throughout the FMR1 knockout mouse brain (data not shown). Due to limited visualization of dendritic staining, the current study focuses on the description of somatic FMRP staining.

Mouse monoclonal anti-β-actin was used as a loading control in Western blot analysis. This antibody recognizes an epitope located on the N-terminal end of the β-isoform of actin. It

specifically labels β-actin in a wide variety of tissues and species, as tested by Western blot (manufacturer's data sheet) and on mouse brains in the current study.

The optimal antibody concentration was obtained by running a series of concentration tests to avoid floor or ceiling truncation, including a negative control by omitting primary antibody. Immunogen, host species, clone type, manufacturer's information, as well as dilution used for each antibody in each species, are listed in Table 1.

Western blot

Protein samples were harvested from flash frozen brain tissue from wild-type and FMR1 knockout mice. Samples were homogenized in EDTA buffer (62.5 mM Tris-HCl pH 6.8, 2% SDS, 10% Glycerol, 5% β-ME, 10 mM EDTA) using the Ultra-Turrax® T10 homogenizer (IKA® Works, Inc., Wilmington, NC). For each sample, 50 μg of protein in SDS buffer (2% SDS, 50 mM Tris pH 7.6, 5% glycerol, and 0.025% bromophenol blue) was incubated at 70°C for 10 minutes, resolved in NuPAGE 4–12% Bis-Tris Gels (Life Technologies, Carlsbad, CA), and then transferred onto PDVF membranes (GE Healthcare, Chicago, IL). After blocking in 5% milk in PBS with 0.05% Tween (PBS-T) for 30 minutes at room temperature, membranes were probed against a primary anti-FMRP antibody or β-actin for loading control overnight at 4°C in 1% milk in PBS-T. Specific secondary HRP-conjugated antibodies were used at 1:2500 dilution (Santa Cruz, Biotechonology®, Inc., Dallas, TX) and blots were developed with SuperSignal™ West Pico Chemiluminescent Substrate (Thermo Scientific, Inc., Waltham, MA) and exposed to X-ray film.

Data analysis

For each brain, every fourth sections were immunostained for one FMRP antibody, which contained 105–115 coronal sections from the spinal cord to the olfactory bulb or 50–60 parasagittal sections from lateral to the middle line. To avoid staining variations across slides and sections, sections within the same series were treated the same way and simultaneously whenever possible. For each section, image tiles were captured at 16 bits with a 20x lens and an Axiocam 503 color camera mounted on a Zeiss Imager M2 microscope. While imaging, a software Autofocus program in the Zeiss Zen software was applied to ensure all image tiles in focus. The image tiles were then montaged using the titling function of the Zeiss Zen software. This imaging protocol generated a single image of the entire section at a high resolution. All sections were captured and subsequently processed using the same parameters, so that the optic intensity of the background was within 1% deviation across images. Here the background is referred to a region on the slide without brain tissue present. Image brightness and contrast adjustments were performed using Adobe PhotoShop (Adobe System, Mountain View, CA). All drawings were produced in Adobe Illustrator (Adobe System).

All subsequent quantitative analyses were based on measurements from 7G1 immunostaining. To reveal FMRP-rich cells throughout the mouse brain, we performed a pixel-based threshold analysis. The tiled image of an entire section was converted to 8 bit in black and white and used to generate a threshold image at the pixel brightness point of 114

using Fiji software (version 1.50e; National Institute of Health). This threshold was chosen to reveal high intensities of FMRP staining and was applied to all sections analyzed.

To compare FMRP expression levels between cell groups, we performed an intensity analysis on FMRP immunostaining at the individual cell level in eighty-five (85) selected neuronal cell groups. For each cell group, all 7G1-labeled coronal sections containing a significant portion of this cell group were identified. The most middle sections were used to determine the cells to be measured based on the following criteria: 1) its location can be unambiguously identified within the border of the cell group; 2) this cell has an identifiable cell boundary and a well-defined nucleus and; 3) the cross sectional cell body area of this cell is more than 40 μm^2. To analyze a minimum of 30 cells from each cell group, a single section was used for large cell groups while multiple sections were used for smaller cell groups. Once a section was included in the analysis for a particular cell group, all cells matching the above criteria were measured.

For each selected cell, the mean optical intensity of FMRP immunostaining within the cell body was measured in the Fiji software (version 1.50e; National Institute of Health). After background subtraction, the optical intensity of each measured cell was normalized to the average optical intensity of all measured cells in the ventral premammillary nucleus (PMv), the cell group with the smallest average optical intensity among all measured cell groups. The background was measured in a region where there was no tissue present. Statistical analyses between cell groups were performed in the Prism software (Version 6; GraphPad Software, Inc.; La Jolla, CA) using either unpaired student t-test or one-way ANOVA followed with Tukey's multiple comparisons test. Only cell groups presented and measured from the same sections were compared statistically to minimize false positive.

To avoid individual bias in selecting cells to be measured and in outlining the border of the cell body, we selected 13 out of 85 cell groups and had them measured independently by three individual experimenters. The generated three sets of measurements demonstrate similar results in comparing FMRP staining intensity between the 13 cell groups, indicating that individual bias, if any, does not affect the main conclusion of the study. All data presented in the Results and figures are resulted from the measurements from one experimenter.

One consideration is at what degree the cellular quantification performed in the current study represents the entire neuronal population in the mouse brain. The goal of the current study is to provide qualitative and quantitative comparisons of FMRP expression levels across the whole brain from brainstem and midbrain to thalamus and cortex. This breadth of objectives limits the depth of the analyses. First, our description and measurements focus on the most prominent cell groups readily identifiable based on FMRP immunostaining. Therefore, neuronal cell groups that are small or without discrete borders from surrounding areas were not taken into account. Our series of illustrations throughout the entire brain help identify some of these cell groups. Second, many of the cell groups selected for the analyses have heterogeneous internal organization with multiple subdivisions and/or cell types. We did not attempt to differentiate these subdivisions or cell types unless they are readily identifiable and they differ in their FMRP staining pattern. Third, our cell sampling (n = 30–

60 neurons per cell group) is approximately from the middle of each cell group in coronal sections, rather than random sampling from the entire population of the cell group. Finally, to preferentially represent neuronal vs. glial populations, we analyzed cells with a minimal cross sectional cell body area of 40 μm^2. This approach does not take into account neurons of smaller sizes and glial cells of larger sizes. Taken together, our analyses provide a general sampling from these cell groups, with the hope to stimulate more elaborative studies in specific brain areas in conjunction with functional studies.

RESULTS

Characterization of FMRP antibodies

Two monoclonal anti-FMRP antibodies, 7G1 and 2F5, were tested for their specificity of recognizing mouse FMRP in our preparations (Fig. 1). The antigens are located in the N-terminal and exon 11 for 2F5 and 7G1, respectively, both of which are common for the 12 mouse FMRP isoforms identified by Brackett et al. (2013). On Western blots, both antibodies detect FMRP bands on wild-type mouse brain samples (WT in Fig. 1A). These bands are absent on FMR1 knockout mouse brain samples, except for a weak low-molecular band for 7G1 detection (KO in Fig. 1A). The specificity of the two antibodies was further evaluated by immunocytochemistry. Throughout the entire brain of FMR1 knockout mice, no detectable immunostaining was found for 7G1 and 2F5 antibodies (Fig. 1B), except for a strong 7G1 signal in the ependymal and subendymal layers of the lateral ventricle, sometimes called “olfactory ventricle” (Fig. 1C). Consistently, the olfactory ventricle is labeled in the wild-type mouse brain for 7G1 but not for 2F5 (Fig. 1D–E). We conclude that this 7G1 staining in the olfactory ventricle is not specific for FMRP.

Except for the olfactory ventricle, the distribution pattern of the immunostaining is comparable between 7G1 and 2F5 throughout the wild-type mouse brain, consistent with the assumption that both antibodies recognize all major isoforms of the mouse FMRP. With our staining protocol, 7G1 demonstrates a larger dynamic range of immunostaining intensity than 2F5. In other words, 7G1 illustrates differential patterns of FMRP distribution across brain regions in a more dramatic manner. The subsequent description, illustrations, and quantification are thus based on 7G1 immunostaining.

General distribution pattern of FMRP immunoreactivity

The distribution pattern of FMRP (7G1) immunoreactivity is illustrated in a series of low- and high-magnification images. Figures 2–4 illustrate FMRP staining on three parasagittal sections as well as Nissl stain on adjacent sections. Figures 5–14 illustrate FMRP staining on twelve coronal sections from caudal (the spinal cord) to rostral (the olfactory bulb). Each figure contains the original photomicrograph and the threshold image of FMRP staining. This pixel-based threshold analysis reveals the cells with high FMRP levels. A list of the most prominent FMRP-rich neuronal cell groups is summarized in Table 2. Cellular quantification analyses on eighty five (85) selected neuronal cell groups are demonstrated in Figure 15. High-magnification images of selected brain areas are subsequently provided in Figures 16–27.

For naming individual neuronal cell groups, we adopt the nomenclature of the Allen Mouse Brain Atlas (http://atlas.brain-map.org). For identifying the rostral-caudal and the lateral-medial levels of the illustrated images, we compare our sections with the Mouse Brain Atlas (Paxinos and Franklin, 2013). For the purpose of description, we divide the mouse brain into seven major portions: 1) the brainstem, 2) the midbrain, 3) the cerebellum, 4) the thalamus, 5) the hypothalamus, 6) the cerebral cortex which contains the isocortex, hippocampus, olfactory bulb, and cortical subplate, and 7) the cerebral nuclei which contains striatum and pallidum (see Fig. 2B).

Based on low-magnification images, although FMRP immunoreactivity is presented throughout the entire brain, the intensity of FMRP staining varied largely across brain regions. Consistent with a previous study (Hinds et al., 1993), the most prominent FMRP staining at the low-magnification is seen in the olfactory bulb, isocortex, hippocampus, thalamus, and cerebellum (Fig. 2A). In contrast, the staining level is generally low in the hypothalamus and midbrain. The entire thalamus stands out with high and relatively uniform levels of FMRP immunoreactivity, surrounded by the generally pale staining in the hypothalamus and midbrain (Figs. 2–3, 9–11). The brainstem, which contains a low density of neuronal cell bodies and a large number of axonal fibers as demonstrated by Nissl stain (Fig. 2B), is characterized with many distinct FMRP-rich cell groups.

At the cellular level, FMRP is most extensively localized in the cytoplasm of cell bodies. Labeled cell bodies vary largely in their size. It is a reasonable assumption that the majority of small cell bodies in the white matter are glial cells, while large cell bodies in the grey matters are mostly neuronal. In general, FMRP staining intensity is consistently low in the white matter. The subsequent description focuses on FMRP distribution pattern in the grey matter with respect to individual cell groups listed in the brain atlas. These cell groups are commonly called nuclei or neuronal cell groups as they are generally identified based on packaging patterns of neuronal cell types. Within individual neuronal cell groups, we did not attempt to differentiate glial or neuronal cells. Our cellular quantification analyses include only labeled cell bodies larger than 7 μm in diameter, which excludes a large percentage of glial cells and thus preferentially represents neuronal population.

FMRP staining in the brainstem and spinal cord

Our samples include only the most rostral portion of the spinal cord containing C1–2 segments. In this portion, the spinal cord contains FMRP-rich cells of various sizes throughout the grey matter (Fig. 16A). Labeled cells were detected in both dorsal and ventral horns, indicating that both sensory and motor neurons contain FMRP. A group of large cells display particularly intense staining in the ventral horn (Fig. 16B, arrows), intermixing with cells with relatively lighter staining (Fig. 16B, arrowheads). The white matter of the spinal cord contains weakly labeled small cells, presumably glial cells (Fig. 16C, arrowheads).

In the caudal brainstem, the inferior olive complex (IO), the magnocellular part of the lateral reticular nucleus (LRNm), the nucleus raphe pallidus and obscurus (RPA and RO), the external cuneate nucleus (ECU), and the dorsal motor nucleus of the vagus nerve (DMX), stand out prominently with a remarkably high intensity of FMRP staining (Fig. 17A–I). Darkly labeled cells are also found in the gracile nucleus (GR), the cuneate nucleus (CU),

the giganticellular reticular nucleus (GRN), the abducens nucleus (VI), the facial motor nucleus (VII), and the spinal nucleus of the trigeminal (SPV). The SPV contains several subdivisions with a wide span along the rostrocaudal dimension. FMRP-rich cells are detected throughout this complex, mixed with cells with relatively low intensities of FMRP immunoreactivity. Similarly, the reticular nucleus contain both darkly and weakly labeled cells. In contrast, most cells are weakly labeled in the hypoglossal nucleus (XII) and the nucleus of the solitary tract (NTS), which are immediately adjacent to DMX (Fig. 17J–K). Quantification analysis confirms a significantly higher intensity of FMRP immunoreactivity in DMX than XII at the individual cell level ($p < 0.0001$; Fig. 15A).

At more rostral levels where the vestibulocochlear nerve arrives, auditory nuclei exhibit high levels of FMRP, including the dorsal and ventral portions of the cochlear nucleus (DCO and VCO; Fig. 18A), the superior olivary complex (SOC; Fig. 18E), the nucleus of the trapezoid body (NTB; Fig. 18E), and the nucleus of the lateral lemniscus (NLL; Fig. 18B). The two portions of the cochlear nucleus, DCO and VCO, exhibit different staining patterns. VCO contains distinct darkly labeled cell bodies throughout the nucleus, while cells in DCO are more closely packed and exhibit a wide range of FMRP staining intensity. The intensity of FMRP immunostaining is significantly higher in VCO than in DCO ($p < 0.0001$; Fig. 15A). Differential FMRP staining pattern is also seen between SOC and NTB. The staining intensity of NTB cells appears higher than that of the adjacent SOC nuclei including the lateral superior olive (LSO), the medial superior olive (MSO), and the superior paraolivary nucleus (SPO). This observation is confirmed with quantitatively comparison between NTB and LSO ($p < 0.05$; Fig. 15A). Similarly, FMRP intensity in the vestibular nuclei is not uniform. The medial portion of the vestibular nucleus (MV) shows lower FMRP staining intensities than the lateral, superior, and spinal portions (LAV, SUV, and SPIV; Fig. 18C–D). These differences are statistically significant ($p < 0.01$–0.0001; Fig. 15A).

The most rostral portion of the brainstem is largely occupied by the pontine reticular nucleus (PRN). PRN is low in FMRP immunostaining in general although scattered neurons with strong labeling are also found (Fig. 7). The tegmental reticular nucleus (TRN) and the pontine gray (PG) are heavily loaded with FMRP, in high contrast to the surrounding areas in the brainstem and midbrain (Fig. 19A). The principal sensory nucleus of the trigeminal (PSV) and the motor nucleus of trigeminal (V) also contain a high density of FMRP-rich cells (Fig. 19B). It is interesting to note a group of intensively stained cells embedded in the motor root of the trigeminal nerve. These cells are smaller and more darkly labeled than the cells in the adjacent motor nucleus of trigeminal (Figs. 15B, 19B).

FMRP staining in the midbrain

FMRP staining is generally low in the midbrain. Nevertheless, a number of cell groups containing substantial FMRP immunoreactivity are detected. First, cells in both the external and central nuclei of the inferior colliculus (ICe and ICc) are darkly labeled with comparable staining intensities (Fig. 15A, 20A-C). In contrast, cells in the adjacent periaqueductal gray (PAG) are weakly labeled (Fig. 20D). Second, the large cells of the midbrain trigeminal nucleus (MEV) show strong staining, among the darkest cells for FMRP immunostaining in the entire brain (Figs. 15, 20D). Third, the intermediate gray layer of the superior colliculus

(SCig) exhibit a uniquely strong staining for FMRP (Fig. 20E–F), as compared to other SC layers above and below ($p < 0.0001$; Fig. 15B). Fourth, most cells in the parabigeminal nucleus (PBG) exhibit distinctly high levels of FMRP immunostaining (Fig. 20G). FMRP intensity in PBG is significantly higher than that in SCig ($p < 0.0001$; Fig. 15B). Finally, darkly labeled cells are detected in the compact part of the substantia nigra (SNc; Fig. 19C) and the red nucleus (RN; Fig. 2).

FMRP staining in the thalamus

The entire thalamus displays high and relatively uniform levels of FMRP immunoreactivity. Notably, differential FMRP intensities are detected in two thalamic areas. The first differential pattern is seen in the lateral geniculate complex (LG). The ventral LG division (LGv) and the intergeniculate leaflet (IGL) show significantly lower FMRP staining intensities than the dorsal LG division (LGd; Fig. 21A–C; $p < 0.001$–0.0001; Fig. 15D). The second differential pattern is seen in the epithalamus where the lateral habenula (LH) is stained notably lighter than the medial habenula (MH; Fig. 21D). However, cellular quantification reveals no significant difference in FMRP intensity of individual cell bodies between MH and LH ($p = 0.10$; Fig. 15D), indicating that the stronger staining in MH is primarily due to a higher cell density in MH rather than higher FMRP intensities of individual cell bodies (Fig. 21E–F). Nonetheless, FMRP intensity in both MH and LH are significantly lower than that in the ventrally located parafasciular nucleus (PF; $p < 0.001$; Figs. 15D, 21D).

FMRP staining in the hypothalamus

In contrast to the adjacent thalamus, the hypothalamus exhibits strikingly lower FMRP intensity in most areas. A number of cell groups in the mammillary body, however, show strong FMRP immunostaining, including the lateral mammillary nucleus (LM; Fig. 22A), the ventral part of the tuberomammillary nucleus (TMv; Fig. 22B), and the medial part of the medial mammillary nucleus (MMm; Fig. 22D). In contrast, FMRP staining is weak in the adjacent ventral premammillary nucleus (PMv; Fig. 22F). Additional hypothalamic nuclei containing darkly labeled cells for FMRP are the dorsomedial nucleus of the hypothalamus (DMH, Fig. 22C), the tuberal nucleus (TU; Fig. 22E), the parasubthalamic nucleus (PSTN, Fig. 22G), and the subthalamic nucleus (STN; Fig. 22H).

FMRP staining in the cerebellum

Purkinje neurons at the interface between the granular and the molecular layers of the cerebellum have been reported as one of the neuronal cell types that are most reactive to FMRP immunocytochemistry (Devys et al., 1993). Here we show, the average staining intensity within the cell bodies of the purkinje neurons is medium to strong (Figs. 15B, 23A). Prominent staining is also seen in the granular layer, which consists of small neurons, while in the molecular layer, only few cells show strong labeling. Cells in the three cerebellar nuclei, the fastigial nucleus (FN), interposed nucleus (IP), and dentate nucleus (DN) are stained strongly at comparable levels (Figs. 15B, 23B).

FMRP staining in the cerebral cortex – isocortex

Throughout the entire isocortex, intense FMRP staining is seen in almost all areas and in every layer. Careful examination with high power images, however, reveals heterogeneous internal patterns of FMRP distribution within specific isocortex areas. For example, in the rostral portion of the primary somatosensory cortex, small granular cells in the layer 4 exhibit notably lower FMRP intensities as compared to other layers, while cells in the layers 2–3 appear more darkly labeled than other layers (Fig. 24A). A more dramatic pattern of low FMRP intensities of layer 4 granular cells is seen in the retrosplenial area in particular its ventral part (RSPv), which is called the area 29 (Fig. 24B). In contrast, cells in the layer 4 of the visual area exhibit similar levels of staining as compared to other layers of the same area (Fig. 24C). As another example of heterogeneous FMRP distribution in the isocortex, a unique group of neurons with particularly intense FMRP staining are found in the anterior cingulate area (ACA; Fig. 24D). These cells span the layers 2/3 and 5 but are not usually found in the layer 6. These cells are among the most darkly stained cells in the entire brain. At the level of caudal cortex, it is also noted that FMRP staining intensity is generally lower in the parasubiculum (PAR), postsubiculum (POST), and presubiculum (PRE), than other cortical areas (Fig. 8).

We quantified FMRP intensity at the individual neuron level in four isocortical areas using one-way ANOVA followed with Tukey's multiple comparisons (Fig. 15C). The intensities of FMRP immunoreactivity are significantly different between layers within each cortical area ($p < 0.0001$). Subsequent comparisons further reveal that the layer 4 in the area 29 of the retrosplenial area has significantly lower intensity in FMRP than any other layers ($p < 0.0001$). In addition, FMRP intensity in the layer 6a is significantly lower than the adjacent layers 5 and 6b ($p < 0.01$–0.0001). In the primary visual cortex, cells in the layers 1 and 6b have significantly higher FMRP intensities than other layers ($p < 0.0001$). As expected, the layer 4 of the primary somatosensory cortex at the level of the major body of the caudoputamen, shows significantly lower FMRP intensity than the layers 1, 2/3, and 5 ($p < 0.0001$), but not the layers 6a and 6b. Similar to the somatosensory area, the anterior cingulate area (ACA) shows lower FMRP staining in the deep layers 5 and 6 than the more superficial layers 1–3. As expected, FMRP intensity of the darkly labeled cells (DN in Fig. 15C) spanning the layers 2–5 is significantly higher than any other layers of this cortical region ($p < 0.01$–0.0001).

FMRP staining in the cerebral cortex – cortical subplate

The cortical subplate contains the cell groups in the ventral and adjacent medial to the cortical isocortex, including the claustrum (CLA), the endopiriform nucleus (EP), and several amygdalar nuclei. FMRP immunostaining is strong in most of these cell groups except of the posterior amygdalar nucleus (PA) and the anterior portion of the basomedial amygdalar nucleus (BMAa; Fig. 25). Cellular quantification confirms that FMRP intensity in PA is significantly lower than the adjacent basolateral amygdalar nucleus (BLA; $p < 0.0001$; Fig. 15B), and FMRP intensity in BMAa is significantly lower than the posterior BMA (BMAp; $p < 0.0001$; Fig. 15B).

FMRP staining in the cerebral cortex – hippocampus and olfactory bulb

In all regions of the hippocampus, the pyramidal layer of the CA1–3 and the granule cell layer of the dentate gyrus exhibit strong FMRP staining (Fig. 26). In particular in the CA1, FMRP immunoreactivity accumulates intensively in the ventral portion of the pyramidal cell bodies, giving rise to a dark line in FMRP staining at the interface of the pyramidal layer and the stratum radiatum layer (Fig. 26A). This dark line is not seen in other regions of the hippocampus including the CA3 and the dentate gyrus (Fig. 26B–C). FMRP can also be detected in the proximate portion of the dendrites extending from the CA1 pyramidal layer (arrows in Fig. 26A). In addition, darkly labeled cells were found scattered in other layers of the hippocampus, including the stratum oriens and radiatum layers of the CA1–3, as well as the molecular and polymorph layers of the dentate gyrus (Fig. 26A–C).

All portions of the olfactory area are rich in FMRP immunoreactivity, including the main olfactory bulb (MOB), the accessory olfactory bulb (AOB), the anterior olfactory nucleus (AON), the piriform area (PIR), the cortical amygdalar area (COA), and the nucleus of the lateral olfactory tract (NLOT; Fig. 14C–D). Within the MOB, the staining intensity of the cell bodies is lower in the glomerular layer than the mitral layer (Fig. 15D, 26D).

FMRP staining in the cerebral nuclei – striatum and pallidum

The cortical nuclei contain two major groups, the striatum and pallidum. Most cells in the two groups contain FMRP immunoreactivity at low to medium levels. The caudoputamen (CP), the largest striatum cell group, is clearly less stained than the adjacent isocortex and the cell groups in the cortical subplate (Fig. 15B, 25E–G, 27A–B). Nonetheless, cells are more darkly stained in CP in general than the nucleus accumbens (ACB) and the fundus of striatum. Within the lateral septal complex, the caudodorsal part of the lateral septal nucleus (LSc) exhibits notably higher FMRP intensities than other cell groups of the complex (Fig. 11). Among the striatum-like amygdalar nuclei, the central and medial amygdalar nuclei (CEA and MEA) exhibit low levels of staining, while the intercalated amygdalar nucleus (IA) contains prominent FMRP staining (Fig. 25D–G and 27F). All layers of the olfactory tubercle (OT) are rich in FMRP immunoreactivity, including the embedded islands of Calleja (Figs. 12–14, 27C). In the pallidum, the most prominent FMRP-rich cells are found in the globus pallidus (GP) and the diagonal band nucleus (NDB; Fig. 27D–E).

DISCUSSION

In this study, we provide the first systematic map of cellular distribution of fragile X mental retardation protein (FMRP) throughout the mammalian brain. We describe here that FMRP expression level is highly differential among individual neuronal cell groups in young mature brains. This finding leads to important implications regarding FMRP function in normal brains and sheds light on understanding the pathology of the fragile X syndrome (FXS).

Differential expression of FMRP in young mature brains

There are two current notions regarding the expression pattern of FMRP in the mammalian brain. The first notion is that FMRP expression is high in some brain areas and low in other

regions (Abitbol et al., 1993; Devys et al., 1993; Hinds et al., 1993; Khandjian et al., 1995; Verheij et al., 1995). This “regional distribution” pattern has led to extensive studies of FMRP function in brain regions with high overall FMRP levels, such as the hippocampus and cortex. The second notion considers FMRP expression at the individual cell level and emphasizes that many neuronal types throughout the brain are as intensely stained for FMRP as the neurons in the hippocampus (Feng et al., 1997; Christie et al., 2009). This “universal distribution” concept argues that strong FMRP signals in some brain regions such as the hippocampus may be related to neuron size and density. This notion is supported by accumulating evidence of altered neuronal structure and function throughout the brain following FMRP loss or reduction, including the brainstem (Brown and Kaczmarek, 2011; Rotschafer et al., 2015) and thalamus (Kogan et al., 2004a).

Using systematic mapping of FMRP immunoreactivity in the entire brain and quantitative analyses at the individual cell level, the current study confirms the widespread distribution of FMRP-rich cells throughout the mammalian brain. More importantly, this study demonstrates a highly differential pattern of FMRP expression with regard to individual neuronal cell groups. In almost all major brain areas from the brainstem and midbrain to the thalamus and forebrain, cell groups high in FMRP expression are found located adjacent to cell groups low in FMRP expression. One of the most striking example is that FMRP expression level can differ notably between layers of the same cortical areas and between adjacent cortical areas of the same layers. The overall strong FMRP signal seen in the cortex and hippocampus is partially due to relatively higher percentages of neurons (and probably large glial cells) rich in FMRP in these areas than in other brain regions, in addition to the size and density of general neuronal population as suggested by Feng and his colleagues (1997).

It is interesting to speculate the relationship of FMRP expression with other cellular properties in mature neurons. Clearly, FMRP expression level of a neuron is not simply related to its general function. In the spinal cord and brainstem, both sensory and motor neurons contain high levels of FMRP, and equally important, not all nuclei involved in sensory processing and motor control express high levels of FMRP (see more discussion below). Consistently, sensory neurons in the thalamus express comparable levels of FMRP to most cortical and hippocampal neurons for cognitive and memory processing. In particular, two nuclei located adjacent to each other and involved in similar functional operations can vary dramatically in the level and pattern of FMRP expression. Examples include the dorsal and ventral portions of the cochlear nucleus, the primary targets of auditory nerve from the inner ear (Brown and Ledwith, 1990), as well as the anterior and posterior portions of the basomedial amygdalar nucleus, which both are a part of fear response pathway (Rosen, 2004).

FMRP expression is not specific to the type of neurotransmitters a neuron releases or to the expression of a number of biomarkers that characterize specialized neuronal cell types. FMRP level is comparably high between principle neurons of the medial nucleus of the trapezoid body that release glycine (Bledsoe et al., 1990), hippocampal pyramidal neurons that use glutamate as a neurotransmitter (Deng et al., 2013) and GABAergic Purkinje neurons in the cerebellum (ref). Similarly, nearly all neurons in the inferior olive strongly

express both FMRP and calbindin (Yu et al., 2014), while the cerebellar molecular layer contains numerously darkly labeled small granular cells for FMRP, mostly known to be calbindin negative (Schwaller et al., 2002). This broad overlap of FMRP expression with neuronal function and other cellular properties, along with the differential pattern of FMRP between individual cell groups, highlight the importance of FMRP signal in a wide range but highly selected brain activities. Exploring the underlying mechanisms of this selection is expected to dramatically enhance our understanding of FMRP regulation in the brain.

Implications to FMRP function and FXS pathology

If a cell is normally rich in FMRP, this cell is reasonably expected to have an increased susceptibility to the loss or reduction of this protein, as compared to other cells that require lower levels of FMRP for their healthy function. It is important to note that the distribution pattern of FMRP described here is in young mature brains of 5–6 weeks old mice. Although FMRP expression in the brain begins early in development and continues throughout life (Hinds et al., 1993), FMRP level appears to be associated with specific developmental events (Tessier and Broadie, 2008; Cook et al., 2011; Gholizadeh et al., 2015). Special care should be taken when attempting to associate the distribution pattern of FMRP in mature brains to structural, physiological and behavioral abnormalities found in FXS patients and FMR1 knockout animals. These abnormalities are accumulated consequences of constitutive FMRP reduction during the entire development and acute influence of insufficient FMRP regulation after mature. Furthermore, FMRP has been proposed to play distinct functions at specific developmental stages, from regulating neuronal differentiation during early development, mediating dendritic and synaptic pruning later in development and to controlling activity-dependent neuronal plasticity after mature (Till, 2010; Telias et al., 2013; Chaudhury et al., 2016). Below we discuss how FMRP expression levels in mature brains might be associated with physiological and behavioral studies in FXS patients and animals, with an emphasis on activity dependent neuronal plasticity. This discussion is focused on three brain areas of high interest.

Subcortical sensory processing

Sensory information processing has recently been receiving an increasing amount of attention in studying FXS pathology in humans and animal models (Sinclair et al., 2016). Abnormal sensory processing is common not only to individuals with FXS but also to autism spectrum disorders in general. One novel finding of this current study is the identification of a large number of cell groups with strong FMRP expression in the brainstem, midbrain, and thalamus. Many of these cell groups are involved in fundamental sensory (particularly auditory and visual) information processing and motor control. In contrast, many other subcortical cell groups express relatively low levels of FMRP, indicating that FMRP expression is selectively strong in subcortical sensory and motor neurons. What is equally important to note is that not all sensory and motor neurons at these subcortical levels are normally rich in FMRP. Most auditory nuclei in the brainstem, midbrain, and thalamus strongly express FMRP. Visual nuclei, on the other hand, exhibit a more selected manner of FMRP expression. As consistent with a previous study in primates (Kogan et al., 2004a), high levels of FMRP are seen in the mouse dorsolateral geniculate nucleus, the major thalamic target of the ascending pathway from the retina. FMRP

intensity, however, is relatively low in the superficial layers of the superior colliculus, the major retinal target in the midbrain (Butler et al., 2011). Similarly, not all motor neurons are normally rich in FMRP. Striking difference in FMRP level was seen between the adjacent dorsal motor nucleus of the vagus nerve (DMX) and the hypoglossal nucleus (XII), although both nuclei are the primary cell groups of cranial nerves. Taken together, these observations strongly implicate the importance of FMRP regulation in selected aspects of fundamental sensory information processing in mature brains.

Supportively, subcortical neuronal circuits for information processing are dynamic in response to sensory experiences or to changes in the integrity of periphery sensory inputs. Language or auditory experience shapes pitch processing of auditory neurons in the brainstem (Krishnan and Gandour, 2014) and midbrain (Gao and Suga, 2000). Hearing loss leads to extensive alternations in cellular properties of auditory neurons at both subcortical and cortical levels (Ryugo, 2015; Bayat et al., 2016). In FMR1 knockout mice, altered synaptic connectivity and reduced activity-dependent regulation of ion channel expression and conductance were found in auditory brainstem neurons (Brown and Kaczmarek, 2011; Rotschafer et al., 2015). In light of these studies, we propose that there are two levels of abnormalities at the cortical levels where sensory perception is generated: i) local effects of FMRP loss on cortical neurons themselves and; ii) altered sensory information to these cortical neurons ascending from the thalamus as a consequence of malfunctioned sensory neurons in the brainstem, midbrain, and thalamus. Consistent with this are studies in the olfactory system where high FMRP expression is found in the olfactory bulb where primary processing of smell signals take place. Loss of FMRP leads to altered dendritic dynamics in the olfactory bulb (Daroles et al., 2015) and compromised olfactory function (Larson et al., 2008; Sudhakaran et al., 2014; Nitenson et al., 2015). Thus, there is a critical need for restoring normal neuronal function of subcortical sensory and motor neurons in addition to cortical neurons for effectively correcting sensory dysfunction in FXS, as well as related disabilities in learning, social interaction, and language. Moreover, sensory processing circuits at the subcortical levels are better characterized and may be more conserved across species than cortical neural circuits, providing advantageous experimental models for understanding FMRP regulation of sensory processing.

Hypothalamus

The hypothalamus is in general low in FMRP in mature brains with the exception of a number of cell groups of the mammillary body. The mammillary body is closely related to the hippocampus and plays an important role in spatial memory (Vann and Nelson, 2015). The finding of high FMRP level in the mammillary body is of particular interest in light of memory and learning deficits in FXS individuals and extensive documentation on reduced neuronal plasticity of hippocampal neurons in FMR1 knockout mice (Mercaldo et al., 2009). The current study found varied FMRP expression levels among distinct cell groups of the mammillary body, suggesting differential contribution of each cell group to memory deficits in FXS.

Data on neuroendocrine function of the hypothalamus are seemingly disparate. Hypothalamic nuclei are known to control food intake, body temperature, fatigue, sleep, and

circadian rhythms (Bakos et al., 2016). A number of neuroendocrine studies implicated hypothalamic dysfunction in FXS, including abnormal activation of the hypothalamic-pituitary-adrenal axis (Hessl et al., 2004). In addition, significantly reduced neuronal activity was reported in the hypothalamus of FMR1 knockout mice of 5 weeks old mice (Michalon et al., 2013). These studies may help to explain the abnormal stress responses, sleep abnormalities, and physical growth patterns commonly seen in affected individuals (Bregman et al., 1990; Hessl et al., 2004). Low FMRP expression in most hypothalamic nuclei at the comparable ages is inconsistent with these behavioral studies. Alternatively, it may suggest the importance of FMRP to hypothalamus during development rather than at relatively more mature stages. Consistently, significant increased grey volume in hypothalamus was found in 1–3 years old kids with FXS (Hoeft et al., 2008) but not in older children (Gothelf et al., 2008). It is clear that further research is needed to consolidate these seemingly disparate findings, but it does raise the possibility that FMRP may express at different levels in developing hypothalamic nuclei.

Cortex layer 4

Reduced neuronal plasticity of various cortical cell types is repeatedly reported in FMR1 knockout animals (ref). Consistently, FMRP is strongly expressed in almost all layers throughout the neocortex in mature brains. However, FMRP protein level is not uniform as previously considered. One most distinct variation is small granule neurons of the layer 4, the primary cortical targets of ascending thalamic inputs. These small cells exhibit significantly lower FMRP levels as compared to other layers in the area 29 and some somatosensory areas. Interestingly, layer 4 is uniquely highly developed in the area 29 with a corresponding degeneration of layers 2 and 3 (Brodmann, 1909). The area 29, as a portion of the retrosplenial cortex, is thought to participate in memory, navigation, and other cognitive functions (Vann et al., 2009). In the somatosensory area, Till et al. (2012) reported alterations in dendritic and spine morphology of spiny stellate neurons of the layer 4. Whether structural changes occur to small granule cells in the same layer is unknown, probably due to the difficulty of studying this cell type (see discussion in Wang et al., 2010). Layer-specific expression of FMRP is also found in another laminar structure, the superior colliculus. Although the significance and implications of these differential expression patterns in FMRP neurobiology and FXS pathology are unknown, it amplifies the importance of studying FMRP mechanisms with the resolution of individual layers and cell types.

Conclusion

The findings presented in this study are critical for understanding FMRP function in mature brain. Characterization of FMRP cellular distribution patterns at critical developmental stages is essential for exploring specific contribution of various FMRP regulatory mechanisms to normal brain function. Our findings emphasize the need and advantages of studying sensory information processing at subcortical levels for understanding FMRP functions in normal and FXS brains.

Acknowledgments

Sponsored by National Institute on Deafness and Other Communication Disorders grant DC-013074.

We would like to thank Mr. Dale Cunningham for his technical support.

Abbreviations

ACA	Anterior cingulate area
ACB	Nucleus accumbens
aco	anterior commissure, olfactory limb
AOB	Accessory olfactory bulb
AON	Anterior olfactory nucleus
BAC	Bed nucleus of the anterior commissure
BLA	Basolateral amygdalar nucleus
BMA	Basomedial amygdalar nucleus
BMAa	Basomedial amygdalar nucleus, anterior part
BMAp	Basomedial amygdalar nucleus, posterior part
CA1	Field CA1
CA3	Field CA3
ccg	Genu of corpus callosum
CEA	Central amygdalar nucleus
CLA	Claustrum
COA	Cortical amygdalar area
CP	Caudoputamen
cst	corticospinal tract
CU	Cuneate nucleus
DCO	Dorsal cochlear nucleus
DG	Dentate gyrus
DMH	Dorsomedial nucleus of the hypothalamus
DMX	Dorsal motor nucleus of the vagus nerve
DN	Dentate nucleus
ECU	External cuneate nucleus

EP	Endopiriform nucleus
fa	corpus callosum, anterior forceps
FN	Fastigial nucleus
fr	fasciculus retroflexus
GP	Globus pallidus
GR	Gracile nucleus
GRN	Gigantocellular reticular nucleus
gVIIn	genu of the facial nerve
IA	Intercalated amygdalar nucleus
IC	Inferior colliculus
ICc	Inferior colliculus, central nucleus
ICe	Inferior colliculus, external nucleus
IGL	Intergeniculate leaflet of the lateral geniculate complex
IO	Inferior olivary complex
IP	Interposed nucleus
IRN	Intermediate reticular nucleus
isl	Islands of Calleja
LA	Lateral amygdalar nucleus
LAV	Lateral vestibular nucleus
LGd	Dorsal part of the lateral geniculate complex
LGv	Ventral part of the lateral geniculate complex
LH	Lateral habenula
LM	Lateral mammillary nucleus
LP	Lateral posterior nucleus of the thalamus
LRNm	Lateral reticular nucleus, magnocellular part
LSc	Lateral septal nucleus, caudal (caudodorsal) part
LSO	Lateral superior olive
LSr	Lateral septal nucleus, rostral (rostroventral) part
LSv	Lateral septal nucleus, ventral part

MARN	Magnocellular reticular nucleus
MEA	Medial amygdalar nucleus
MEApv	Medial amygdalar nucleus, posteroventral part
MEV	Midbrain trigeminal nucleus
MG	Medial geniculate complex
MH	Medial habenula
MM	Medial mammillary nucleus
MMl	Medial mammillary nucleus, lateral part
MMm	Medial mammillary nucleus, medial part
MOB	Main olfactory bulb
MOBgl	Main olfactory bulb, glomerular layer
MOBgr	Main olfactory bulb, granule layer
MOBmi	Main olfactory bulb, mitral layer
MOBopl	Main olfactory bulb, outer plexiform layer
moV	motor root of the trigeminal nerve
MSO	Medial superior olive
MV	Medial vestibular nucleus
NDB	Diagonal band nucleus
NLL	Nucleus of the lateral lemniscus
NLLd	Nucleus of the lateral lemniscus, dorsal part
NLLh	Nucleus of the lateral lemniscus, horizontal part
NLLv	Nucleus of the lateral lemniscus, ventral part
NLOT	Nucleus of the lateral olfactory tract
NTB	Nucleus of the trapezoid body
NTS	Nucleus of the solitary tract
och	optic chiasm
OT	Olfactory tubercle
PA	Posterior amygdalar nucleus
PAG	Periaqueductal gray

PAR	Parasubiculum
PALv	Pallidum, ventral region
PBG	Parabigeminal nucleus
PF	Parafascicular nucleus
PG	Pontine gray
PIR	Piriform area
PMv	Ventral premammillary nucleus
PO	Posterior complex of the thalamus
POST	Postsubiculum
PRE	Presubiculum
PRN	Pontine reticular nucleus
PRP	Nucleus prepositus
PSTN	Parasubthalamic nucleus
PSV	Principal sensory nucleus of the trigeminal
py	pyramid
RN	Red nucleus
RO	Nucleus raphe obscurus
RPA	Nucleus raphe pallidus
RSPd	Retrosplenial area, dorsal part
SC	Superior colliculus
SCig	Superior colliculus, motor related, intermediate gray layer
SCiw	Superior colliculus, motor related, intermediate white layer
SCm	Superior colliculus, motor related
SCop	Superior colliculus, optic layer
SCs	Superior colliculus, sensory related
SCsg	Superior colliculus, superficial gray layer
SCzo	Superior colliculus, zonal layer
SEZ/RC	subependymal zone
SF	Septofrimbrial nucleus

sm	stria medullaris
SNc	Substantia nigra, compact part
SNr	Substantia nigra, reticular part
SOC	Superior olivary complex
SPIV	Spinal vestibular nucleus
SPO	Superior paraolivary nucleus
SPV	Spinal nucleus of the trigeminal
SS	Primary somatosensory area
STN	Subthalamic nucleus
SUM	Supramammillary nucleus
SUV	Superior vestibular nucleus
TMv	Tuberomammilliary nucleus, ventral part
TRN	Tegmental reticular nucleus
TU	Tuberal nucleus
V	Motor nucleus of the trigeminal
VCO	Ventral cochlear nucleus
VENT	Ventral group of the dorsal thalamus
VI	Abducens nucleus
VII	Facial motor nucleus
VIIn	Facial nerve
VIS	Primary visual area
VL	Lateral Ventricle
VNC	Vestibular nuclei
VP	Ventral posterior complex of the thalamus
VPM	Ventral posteromedial nucleus of the thalamus
VTA	Ventral tegmental area
XII	Hypoglossal nucleus

LITERATURE CITED

Abitbol M, Menini C, Delezoide AL, Rhyner T, Vekemans M, Mallet J. Nucleus basalis magnocellularis and hippocampus are the major sites of FMR-1 expression in the human fetal brain. Nat Genet. 1993; 4:147–53. [PubMed: 8348153]

Akins MR, Leblanc HF, Stackpole EE, Chyung E, Fallon JR. Systematic mapping of fragile X granules in the mouse brain reveals a potential role for presynaptic FMRP in sensorimotor functions. J Comp Neurol. 2012; 520:3687–706. [PubMed: 22522693]

Bagni C, Tassone F, Neri G, Hagerman R. Fragile X syndrome: causes, diagnosis, mechanisms, and therapeutics. J Clin Invest. 2012; 122:4314–22. [PubMed: 23202739]

Bakker CE, Verheij C, Willemsen R, Vanderhelm R, Oerlemans F, Vermey M, Bygrave A, Hoogeveen AT, Oostra BA, Reyniers E, DeBoulle K, Dhooge R, Cras P, Van Velzen N, Nagels G, Martin JJ, Dedeyn PP, Darby JK, Willems PJ. Fmr1 knockout mice: a model to study fragile X mental retardation. The Dutch-Belgian Fragile X Consortium. Cell. 1994; 78:23–33. [PubMed: 8033209]

Bakker CE, de Diego Otero Y, Bontekoe C, Raghoe P, Luteijn T, Hoogeveen AT, Oostra BA, Willemsen R. Immunocytochemical and biochemical characterization of FMRP, FXR1P, and FXR2P in the mouse. Exp Cell Res. 2000; 258:162–70. [PubMed: 10912798]

Bakos J, Zatkova M, Bacova Z, Ostatnikova D. The Role of Hypothalamic Neuropeptides in Neurogenesis and Neuritogenesis. Neural Plast. 2016; 2016:3276383. [PubMed: 26881105]

Bayat A, Farhadi M, Emamdjomeh H, Saki N, Mirmomeni G, Rahim F. Effect of conductive hearing loss on central auditory function. Braz J Otorhinolaryngol. 2016 S1808-8694(16)30046-5.

Beebe K, Wang Y, Kulesza R. Distribution of fragile X mental retardation protein in the human auditory brainstem. Neuroscience. 2014; 273:79–91. [PubMed: 24838064]

Bledsoe SC Jr, Snead CR, Helfert RH, Prasad V, Wenthold RJ, Altschuler RA. Immunocytochemical and lesion studies support the hypothesis that the projection from the medial nucleus of the trapezoid body to the lateral superior olive is glycinergic. Brain Res. 1990; 517(1–2):189–94. [PubMed: 2375987]

Brackett DM, Qing F, Amieux PS, Sellers DL, Horner PJ, Morris DR. FMR1 transcript isoforms: association with polyribosomes; regional and developmental expression in mouse brain. PLoS One. 2013; 8:e58296. [PubMed: 23505481]

Braun K, Segal M. FMRP involvement in formation of synapses among cultured hippocampal neurons. Cereb Cortex. 2000; 10:1045–52. [PubMed: 11007555]

Bregman JD, Leckman JF, Ort SI. Thyroid function in fragile-X syndrome males. Yale J Biol Med. 1990; 63(4):293–9. [PubMed: 2125773]

Brodmann, K. Localisation in the cerebral cortex. In: Garey, LJ., translator and editor. The Third Edition. Springer; New York City, NY: 1909.

Brown MC, Ledwith JV 3rd. Projections of thin (type-II) and thick (type-I) auditory-nerve fibers into the cochlear nucleus of the mouse. Hear Res. 1990; 49(1–3):105–18. [PubMed: 1963423]

Brown V, Jin P, Ceman S, Darnell JC, O'Donnell WT, Tenenbaum SA, Jin X, Feng Y, Wilkinson KD, Keene JD, Darnell RB, Warren ST. Microarray identification of FMRP-associated brain mRNAs and altered mRNA translational profiles in fragile X syndrome. Cell. 2001; 107:477–87. [PubMed: 11719188]

Brown MR, Kaczmarek LK. Potassium channel modulation and auditory processing. Hear Res. 2011; 279:32–42. [PubMed: 21414395]

Butler AB, Reiner A, Karten HJ. Evolution of the amniote pallium and the origins of mammalian neocortex. Ann N Y Acad Sci. 2011; 1225:14–27. [PubMed: 21534989]

Chaudhury S, Sharma V, Kumar V, Nag TC, Wadhwa S. Activity-dependent synaptic plasticity modulates the critical phase of brain development. Brain Dev. 2016; 38(4):355–63. [PubMed: 26515724]

Chen L, Toth M. Fragile X mice develop sensory hyperreactivity to auditory stimuli. Neuroscience. 2001; 103:1043–50. [PubMed: 11301211]

Christie SB, Akins MR, Schwob JE, Fallon JR. The FXG: a presynaptic fragile X granule expressed in a subset of developing brain circuits. J Neurosci. 2009; 29:1514–24. [PubMed: 19193898]

Cook D, Nuro E, Murai KK. Increasing our understanding of human cognition through the study of Fragile X Syndrome. Dev Neurobiol. 2014; 74:147–177. [PubMed: 23723176]

Daroles L, Gribaudo S, Doulazmi M, Scotto-Lomassese S, Dubacq C, Mandairon N, Greer CA, Didier A, Trembleau A, Caillé I. Fragile X Mental Retardation Protein and Dendritic Local Translation of the Alpha Subunit of the Calcium/Calmodulin-Dependent Kinase II Messenger RNA Are Required for the Structural Plasticity Underlying Olfactory Learning. Biol Psychiatry. 2015 S0006-3223(15)00642-3.

Devys D, Lutz Y, Rouyer N, Bellocq JP, Mandel JL. The FMR-1 protein is cytoplasmic, most abundant in neurons and appears normal in carriers of a fragile X premutation. Nat Genet. 1993; 4:335–40. [PubMed: 8401578]

Edwards SB, Ginsburgh CL, Henkel CK, Stein BE. Sources of subcortical projections to the superior colliculus in the cat. J Comp Neurol. 1979; 184:309–29. [PubMed: 762286]

Feng Y, Gutekunst CA, Eberhart DE, Yi H, Warren ST, Hersch SM. Fragile X mental retardation protein: nucleocytoplasmic shuttling and association with somatodendritic ribosomes. J Neurosci. 1997; 17:1539–47. [PubMed: 9030614]

Fisch GS, Hao HK, Bakker C, Oostra BA. Learning and memory in the FMR1 knockout mouse. Am J Med Genet. 1999; 84:277–82. [PubMed: 10331607]

Gao E, Suga N. Experience-dependent plasticity in the auditory cortex and the inferior colliculus of bats: role of the corticofugal system. Proc Natl Acad Sci U S A. 2000; 97(22):11807–14. [PubMed: 11050213]

Gabel LA, Won S, Kawai H, McKinney M, Tartakoff AM, Fallon JR. Visual experience regulates transient expression and dendritic localization of fragile X mental retardation protein. J Neurosci. 2004; 24:10579–83. [PubMed: 15564573]

Galvez R, Gopal AR, Greenough WT. Somatosensory cortical barrel dendritic abnormalities in a mouse model of the fragile X mental retardation syndrome. Brain Res. 2003; 971:83–9. [PubMed: 12691840]

Galvez R, Smith RL, Greenough WT. Olfactory bulb mitral cell dendritic pruning abnormalities in a mouse model of the Fragile-X mental retardation syndrome: further support for FMRP's involvement in dendritic development. Brain Res Dev Brain Res. 2005; 157:214–6. [PubMed: 15878626]

Gholizadeh S, Halder SK, Hampson DR. Expression of fragile X mental retardation protein in neurons and glia of the developing and adult mouse brain. Brain Res. 2015; 1596:22–30. [PubMed: 25446451]

Gothelf D, Furfaro JA, Hoeft F, Eckert MA, Hall SS, O'Hara R, Erba HW, Ringel J, Hayashi KM, Patnaik S, Golianu B, Kraemer HC, Thompson PM, Piven J, Reiss AL. Neuroanatomy of fragile X syndrome is associated with aberrant behavior and the fragile X mental retardation protein (FMRP). Ann Neurol. 2008; 63(1):40–51. [PubMed: 17932962]

Graybiel AM. A satellite system of the superior colliculus: the parabigeminal nucleus and its projections to the superficial collicular layers. Brain Res. 1978; 145:365–74. [PubMed: 638795]

Hinds HL, Ashley CT, Sutcliffe JS, Nelson DL, Warren ST, Housman DE, Schalling M. Tissue specific expression of FMR-1 provides evidence for a functional role in fragile X syndrome. Nat Genet. 1993; 3:36–43. [PubMed: 8490651]

Hinton VJ, Brown WT, Wisniewski K, Rudelli RD. Analysis of neocortex in three males with the fragile X syndrome. Am J Med Genet. 1991; 41:289–94. [PubMed: 1724112]

Hessl D, Rivera SM, Reiss AL. The neuroanatomy and neuroendocrinology of fragile X syndrome. Ment Retard Dev Disabil Res Rev. 2004; 10(1):17–24. [PubMed: 14994284]

Hoeft F, Lightbody AA, Hazlett HC, Patnaik S, Piven J, Reiss AL. Morphometric spatial patterns differentiating boys with fragile X syndrome, typically developing boys, and developmentally delayed boys aged 1 to 3 years. Arch Gen Psychiatry. 2008; 65(9):1087–97. [PubMed: 18762595]

Irwin SA, Patel B, Idupulapati M, Harris JB, Crisostomo RA, Larsen BP, Kooy F, Willems PJ, Cras P, Kozlowski PB, Swain RA, Weiler IJ, Greenough WT. Abnormal dendritic spine characteristics in the temporal and visual cortices of patients with fragile-X syndrome: a quantitative examination. Am J Med Genet. 2001; 98:161–7. [PubMed: 11223852]

Irwin SA, Idupulapati M, Gilbert ME, Harris JB, Chakravarti AB, Rogers EJ, Crisostomo RA, Larsen BP, Mehta A, Alcantara CJ, Patel B, Swain RA, Weiler IJ, Oostra BA, Greenough WT. Dendritic spine and dendritic field characteristics of layer V pyramidal neurons in the visual cortex of fragile-X knockout mice. Am J Med Genet. 2002; 111:140–6. [PubMed: 12210340]

Khandjian EW, Fortin A, Thibodeau A, Tremblay S, Côté F, Devys D, Mandel JL, Rousseau F. A heterogeneous set of FMR1 proteins is widely distributed in mouse tissues and is modulated in cell culture. Hum Mol Genet. 1995; 4:783–9. [PubMed: 7633436]

Kogan CS, Bertone A, Cornish K, Boutet I, Der Kaloustian VM, Andermann E, Faubert J, Chaudhuri A. Integrative cortical dysfunction and pervasive motion perception deficit in fragile X syndrome. Neurology. 2004a; 63:1634–9. [PubMed: 15534248]

Kogan CS, Boutet I, Cornish K, Zangenehpour S, Mullen KT, Holden JJ, Der Kaloustian VM, Andermann E, Chaudhuri A. Differential impact of the FMR1 gene on visual processing in fragile X syndrome. Brain. 2004b; 127:591–601. [PubMed: 14736752]

Krishnan A, Gandour JT. Language experience shapes processing of pitch relevant information in the human brainstem and auditory cortex: electrophysiological evidence. Acoust Aust. 2014; 42(3): 166–178. [PubMed: 25838636]

La Fata G, Gärtner A, Domínguez-Iturza N, Dresselaers T, Dawitz J, Poorthuis RB, Averna M, Himmelreich U, Meredith RM, Achsel T, Dotti CG, Bagni C. FMRP regulates multipolar to bipolar transition affecting neuronal migration and cortical circuitry. Nat Neurosci. 2014; 17:1693–700. [PubMed: 25402856]

Lai JK, Lerch JP, Doering LC, Foster JA, Ellegood J. Regional brain volumes changes in adult male FMR1-KO mouse on the FVB strain. Neuroscience. 2016; 318:12–21. [PubMed: 26794591]

Larson J, Kim D, Patel RC, Floreani C. Olfactory discrimination learning in mice lacking the fragile X mental retardation protein. Neurobiol Learn Mem. 2008; 90:90–102. [PubMed: 18289890]

Levenga J, de Vrij FM, Buijsen RA, Li T, Nieuwenhuizen IM, Pop A, Oostra BA, Willemsen R. Subregion-specific dendritic spine abnormalities in the hippocampus of Fmr1 KO mice. Neurobiol Learn Mem. 2011; 95:467–72. [PubMed: 21371563]

McKinney BC, Grossman AW, Elisseou NM, Greenough WT. Dendritic spine abnormalities in the occipital cortex of C57BL/6 Fmr1 knockout mice. Am J Med Genet B Neuropsychiatr Genet. 2005; 136:98–102.

Mercaldo V, Descalzi G, Zhuo M. Fragile X mental retardation protein in learning-related synaptic plasticity. Mol Cells. 2009; 28(6):501–7. [PubMed: 20047076]

Michalon A, Bruns A, Risterucci C, Honer M, Ballard TM, Ozmen L, Jaeschke G, Wettstein JG, von Kienlin M, Künnecke B, Lindemann L. Chronic metabotropic glutamate receptor 5 inhibition corrects local alterations of brain activity and improves cognitive performance in fragile X mice. Biol Psychiatry. 2013; 75(3):189–97. [PubMed: 23910948]

Nitenson AS, Stackpole EE, Truszkowski TL, Midroit M, Fallon JR, Bath KG. Fragile X mental retardation protein regulates olfactory sensitivity but not odorant discrimination. Chem Senses. 2015; 40:345–50. [PubMed: 25917509]

Deng PY, Rotman Z, Blundon JA, Cho Y, Cui J, Cavalli V, Zakharenko SS, Klyachko VA. FMRP regulates neurotransmitter release and synaptic information transmission by modulating action potential duration via BK channels. Neuron. 2013; 77(4):696–711. [PubMed: 23439122]

Paxinos, G., Franklin, KBJ. The Mouse Brain in Stereotaxic Coordinates. 4. Academic Press; Cambridge, MT: 2013.

Penagarikano O, Mulle JG, Warren ST. The pathophysiology of fragile X syndrome. Annu Rev Genomics Hum Genet. 2007; 8:109–29. [PubMed: 17477822]

Pietropaolo S, Guilleminot A, Martin B, D'Amato FR, Crusio WE. Genetic-background modulation of core and variable autistic-like symptoms in Fmr1 knock-out mice. PLoS One. 2011; 6:e17073. [PubMed: 21364941]

Rosen JB. The neurobiology of conditioned and unconditioned fear: a neurobehavioral system analysis of the amygdala. Behav Cogn Neurosci Rev. 2004; 3:23–41. [PubMed: 15191640]

Rotschafer SE, Marshak S, Cramer KS. Deletion of Fmr1 alters function and synaptic inputs in the auditory brainstem. PLoS One. 2015; 10:e0117266. [PubMed: 25679778]

Rudelli RD, Brown WT, Wisniewski K, Jenkins EC, Laure-Kamionowska M, Connell F, Wisniewski HM. Adult fragile X syndrome. Clinico-neuropathologic findings. Acta Neuropathol. 1985; 67:289–95. [PubMed: 4050344]

Ryugo D. Auditory neuroplasticity, hearing loss and cochlear implants. Cell Tissue Res. 2015; 361(1): 251–69. [PubMed: 25300646]

Santoro MR, Bray SM, Warren ST. Molecular mechanisms of fragile X syndrome: a twenty-year perspective. Annu Rev Pathol. 2012; 7:219–45. [PubMed: 22017584]

Schwaller B, Meyer M, Schiffmann S. 'New' functions for 'old' proteins: the role of the calcium-binding proteins calbindin D-28k, calretinin and parvalbumin, in cerebellar physiology. Studies with knockout mice. Cerebellum. 2002; 1(4):241–58. [PubMed: 12879963]

Sinclair D, Oranje B, Razak KA, Siegel SJ, Schmid S. Sensory processing in autism spectrum disorders and Fragile X syndrome-From the clinic to animal models. Neurosci Biobehav Rev. 2016 S0149–7634(15)30318–3.

Strumbos JG, Brown MR, Kronengold J, Polley DB, Kaczmarek LK. Fragile X mental retardation protein is required for rapid experience-dependent regulation of the potassium channel Kv3.1b. J Neurosci. 2010; 30:10263–71. [PubMed: 20685971]

Sudhakaran IP1, Hillebrand J, Dervan A, Das S, Holohan EE, Hülsmeier J, Sarov M, Parker R, VijayRaghavan K, Ramaswami M. FMRP and Ataxin-2 function together in long-term olfactory habituation and neuronal translational control. Proc Natl Acad Sci U S A. 2014; 111:E99–E108. [PubMed: 24344294]

Telias M, Segal M, Ben-Yosef D. Neural differentiation of Fragile X human Embryonic Stem Cells reveals abnormal patterns of development despite successful neurogenesis. Dev Biol. 2013; 374(1):32–45. [PubMed: 23219959]

Tessier CR, Broadie K. Drosophila fragile X mental retardation protein developmentally regulates activity-dependent axon pruning. Development. 2008; 135(8):1547–57. [PubMed: 18321984]

Till SM. The developmental roles of FMRP. Biochem Soc Trans. 2010; 38(2):507–10. [PubMed: 20298211]

Till SM, Wijetunge LS, Seidel VG, Harlow E, Wright AK, Bagni C, Contractor A, Gillingwater TH, Kind PC. Altered maturation of the primary somatosensory cortex in a mouse model of fragile X syndrome. Hum Mol Genet. 2012; 21:2143–56. [PubMed: 22328088]

Thomas CC, Combe CL, Dyar KA, Inglis FM. Modest Alterations in Patterns of Motor Neuron Dendrite Morphology in the Fmr1 Knockout Mouse Model for Fragile X. Int J Devl Neuroscience. 2008; 26:805–811.

Vann SD, Aggleton JP, Maguire EA. What does the retrosplenial cortex do? Nat Rev Neurosci. 2009; 10:792–802. [PubMed: 19812579]

Vann SD, Nelson AJ. The mammillary bodies and memory: more than a hippocampal relay. Prog Brain Res. 2015; 219:163–85. [PubMed: 26072239]

Verheij C, de Graaff E, Bakker CE, Willemsen R, Willems PJ, Meijer N, Galjaard H, Reuser AJ, Oostra BA, Hoogeveen AT. Characterization of FMR1 proteins isolated from different tissues. Hum Mol Genet. 1995; 4:895–901. [PubMed: 7633450]

Verkerk AJMH, Pieretti M, Sutcliffe JS, Fu Y-H, Kuhl DPA, Pizzuti A, Reiner O, Richards S, Victoria MF, Zhang F, Eussen BE, van Ommen GJB, Blonden LAJ, Riggins GJ, Chastain JL, Kunst CB, Galjaard H, Caskey CT, Nelson DL, Oostra BA, Warren ST. Identification of a gene (FMR-1) containing a CGG repeat coincident with a breakpoint cluster region exhibiting length variation in fragile X syndrome. Cell. 1991; 65:905–914. [PubMed: 1710175]

Wang Y, Major DE, Karten HJ. Morphology and connections of nucleus isthmi pars magnocellularis in chicks (Gallus gallus). J Comp Neurol. 2004; 469:275–97. [PubMed: 14694539]

Wang Y, Luksch H, Brecha NC, Karten HJ. Columnar projections from the cholinergic nucleus isthmi to the optic tectum in chicks (Gallus gallus): a possible substrate for synchronizing tectal channels. J Comp Neurol. 2006; 494:7–35. [PubMed: 16304683]

Wang Y, Brzozowska-Prechtl A, Karten HJ. Laminar and columnar auditory cortex in avian brain. Proc Natl Acad Sci USA. 2010; 107:12676–12681. [PubMed: 20616034]

Wang Y, Sakano H, Beebe K, Brown MR, de Laat R, Bothwell M, Kulesza RJ Jr, Rubel EW. Intense and specialized dendritic localization of the fragile X mental retardation protein in binaural

brainstem neurons: a comparative study in the alligator, chicken, gerbil, and human. J Comp Neurol. 2014; 522:2107–28. [PubMed: 24318628]

Zangenehpour S, Cornish KM, Chaudhuri A. Whole-brain expression analysis of FMRP in adult monkey and its relationship to cognitive deficits in fragile X syndrome. Brain Res. 2009; 1264:76–84. [PubMed: 19368811]

Yu Y, Fu Y, Watson C. The inferior olive of the C57BL/6J mouse: a chemoarchitectonic study. Anat Rec (Hoboken). 2014; 297(2):289–300. [PubMed: 24443186]

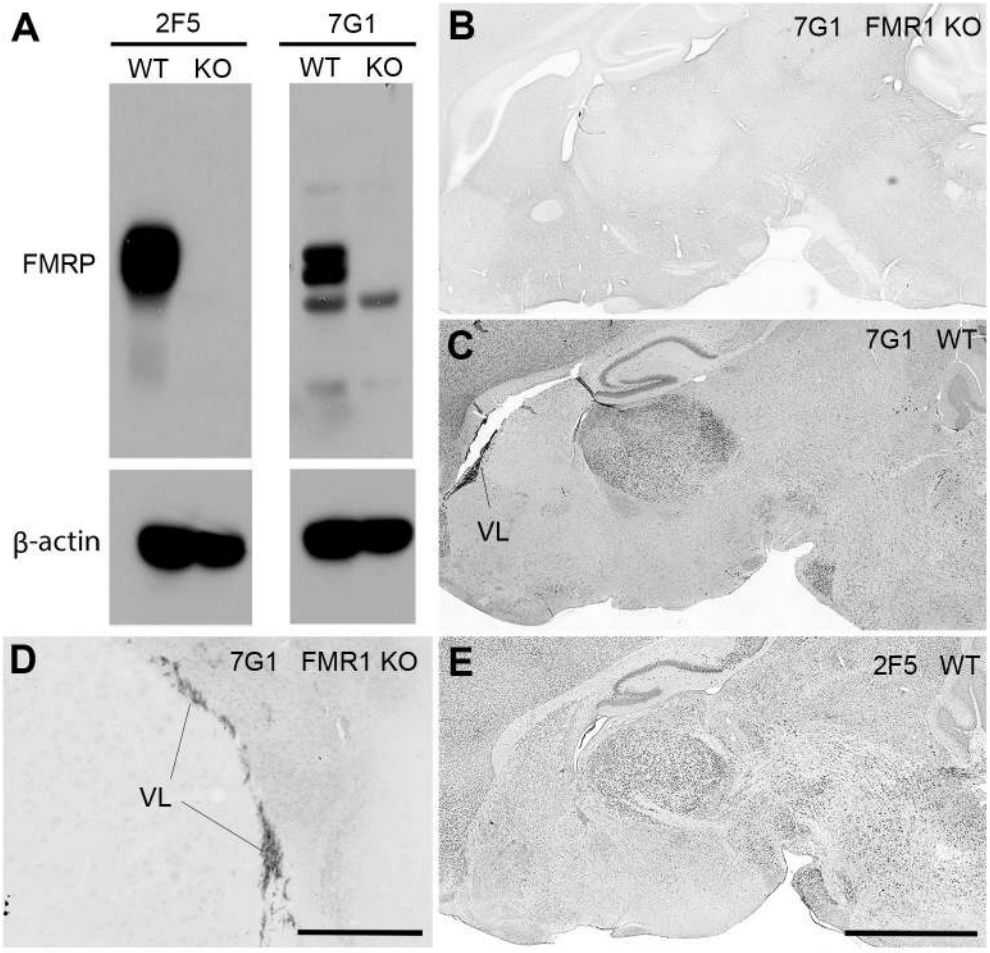

Figure 1.

Antibody characterization for FMRP in the mouse brain. **A,** Western blot of 2F5 and 7G1 on brain samples from wild-type (WT) and FMR1 knockout (KO) mice. 50 μg of protein was loaded to each lane with β-actin as the loading control. **B–D,** 7G1 immunostaining in the WT (**C**) and FMR1 KO (**B, D**) mouse brain. Note the nonspecific staining in the lateral ventricle (VL; **D**). **E,** 2F5 immunostaining in the WT mouse brain. Scale bar: 2 mm (A, B, C, E); 500 μm (D).

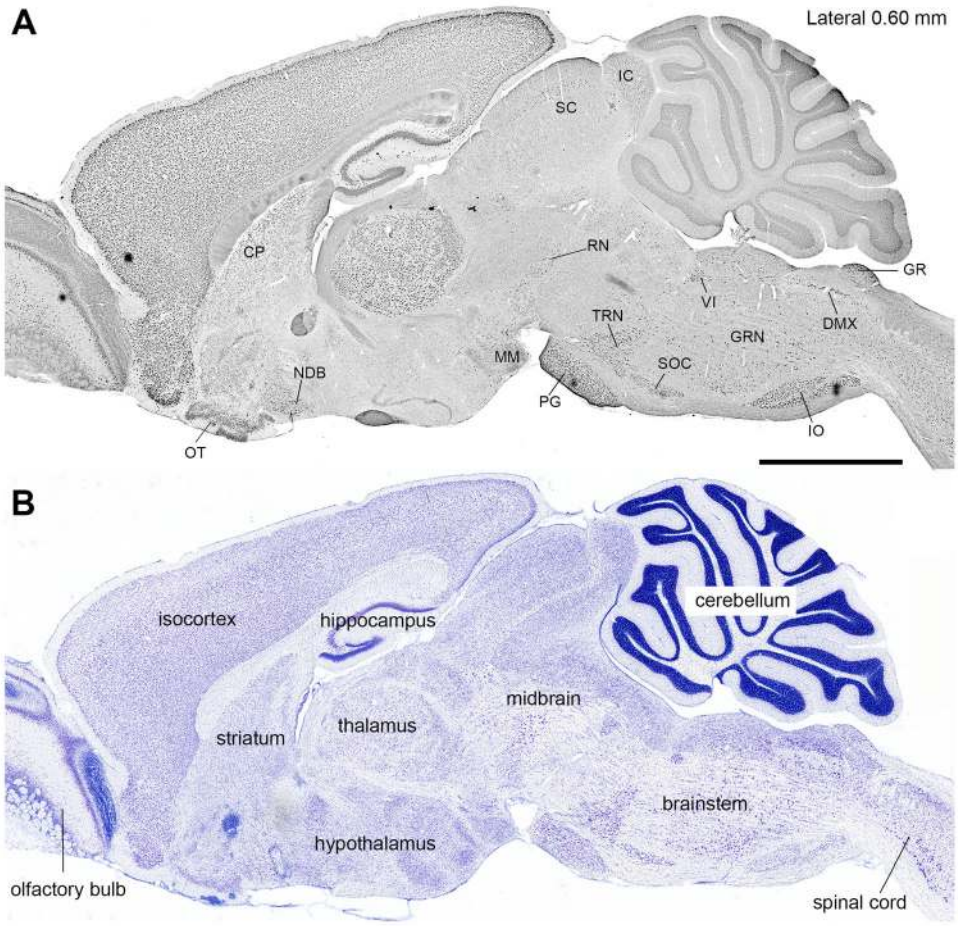

Figure 2.

FMRP (7G1) immunostaining in the sagittal plane at the medial level of the wild-type mouse brain. This level is comparable to Lateral 0.60 mm according to the Mouse Brain Atlas (Paxinos and Franklin, 2013). The 7G1 immunostaining (**A**) and the Nissl stain (**B**) were taken from two sections at the comparable level. Note differential FMRP levels across brain regions, high in the olfactory bulb, cerebral cortex, hippocampus, thalamus, and cerebellum, and generally low in the hypothalamus and midbrain. The brainstem contains many distinct cell groups that are rich in FMRP. Scale bar: 2 mm.

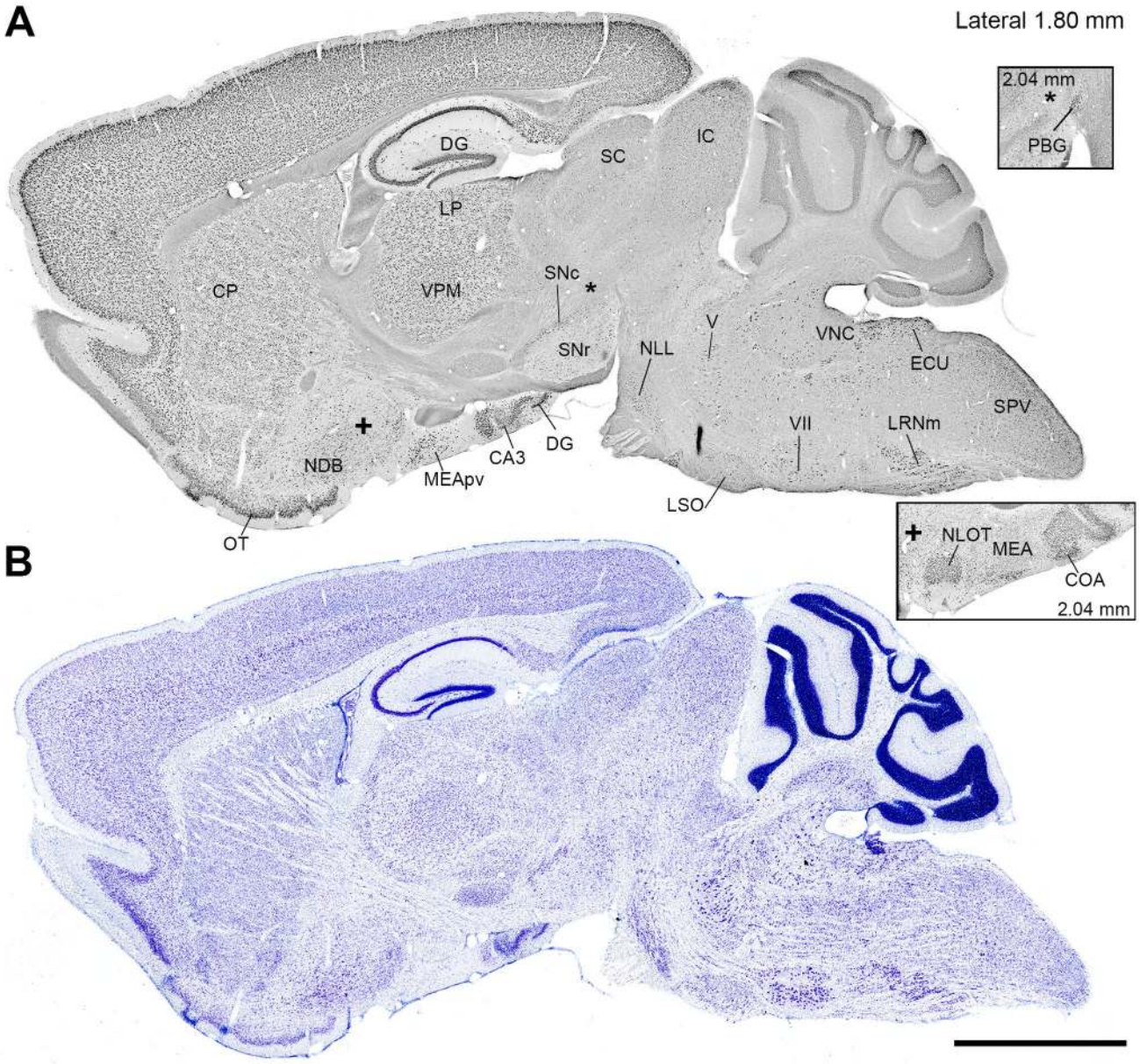

Figure 3.

FMRP (7G1) immunostaining in the sagittal plane at the middle level of the wild-type mouse brain. This level is comparable to Lateral 1.80 mm according to the Mouse Brain Atlas (Paxinos and Franklin, 2013). The 7G1 immunostaining (**A**) and the Nissl stain (**B**) were taken from two sections at the comparable level. The two inserts were taken from a section at the level of Lateral 2.04 mm, corresponding to the location marked with * and $^{+}$, respectively. Scale bar: 2 mm.

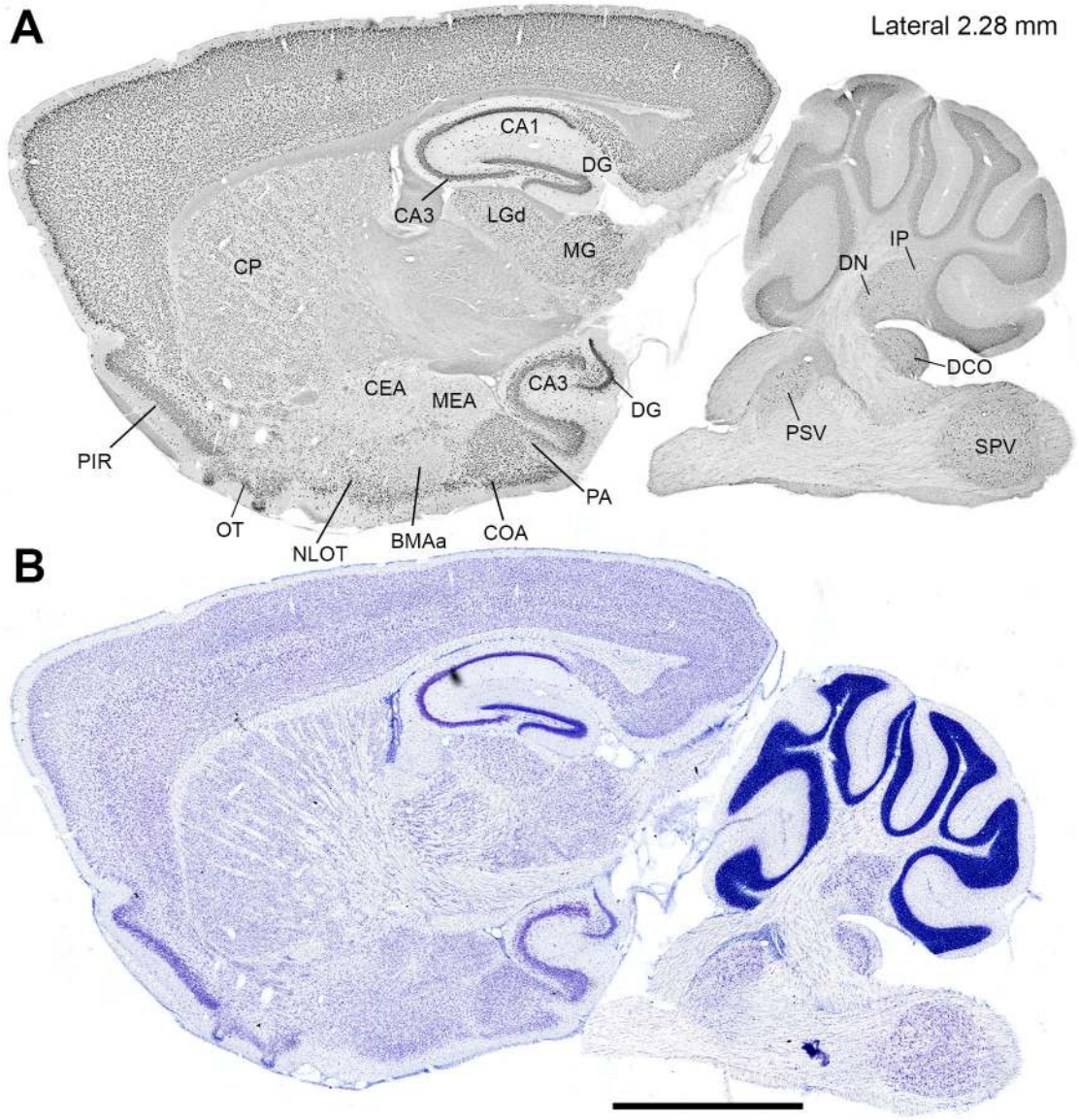

Figure 4.

FMRP (7G1) immunostaining in the sagittal plane at the lateral level of the wild-type mouse brain. This level is comparable to Lateral 2.28 mm according to the Mouse Brain Atlas (Paxinos and Franklin, 2013). The 7G1 immunostaining (**A**) and the Nissl stain (**B**) were taken from two sections at the comparable level. Scale bar: 2 mm.

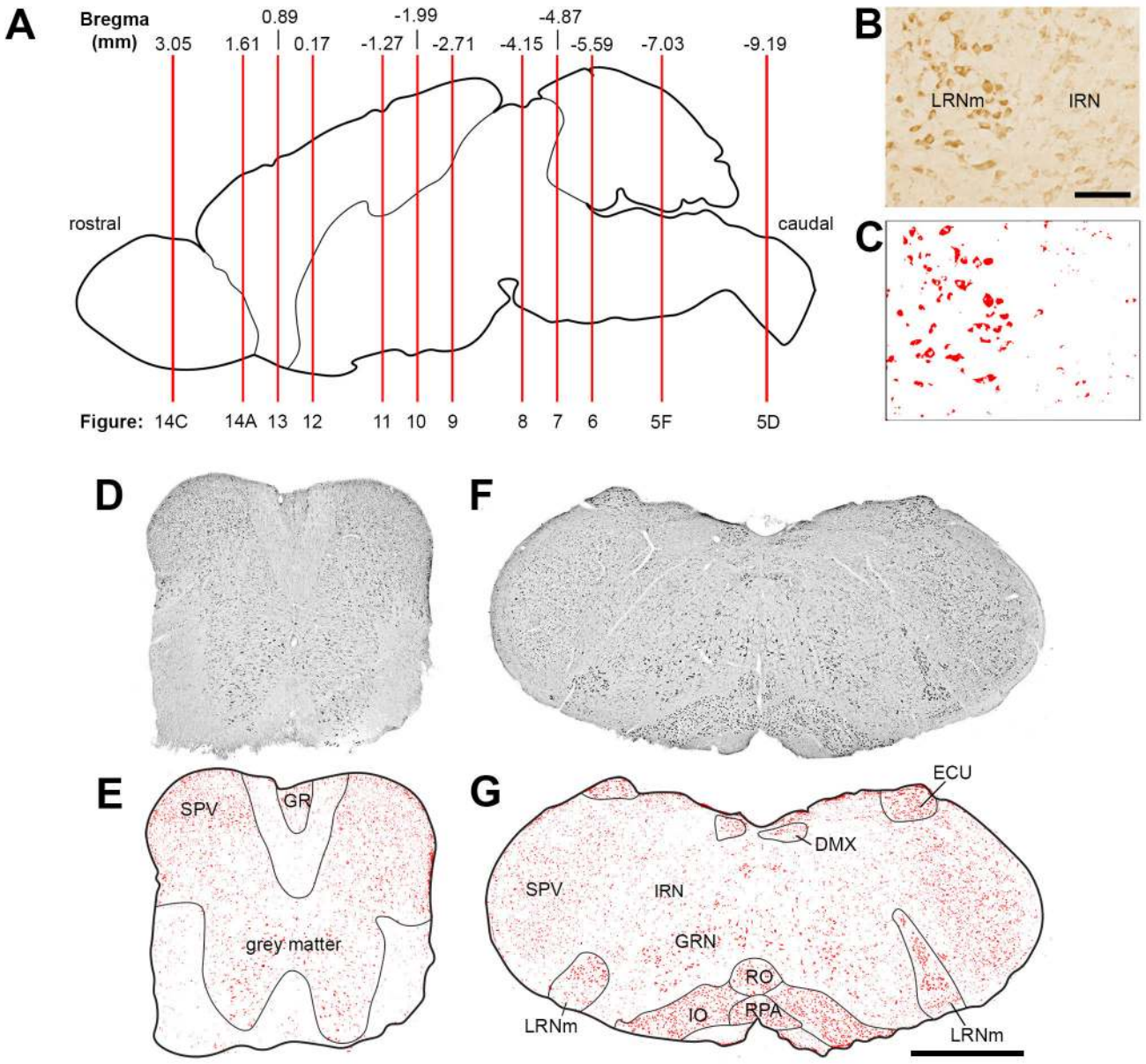

Figure 5.

FMRP (7G1) immunostaining in the coronal plane through the spinal cord and caudal brainstem. **A:** Schematic drawing showing the levels of the coronal sections illustrated in the Figures 5–14 (red vertical lines). The black lines outline the mouse brain in the sagittal plane. The numerical rostral-caudal levels of each section is indicated on the top of the drawing, determined by comparing to the Mouse Brain Atlas (Paxinos and Franklin, 2013). **B–C:** An example of the original image (**B**) and generated threshold image (**C**) at a high magnification. **D–E:** The photomicrograph (**D**) and the threshold image (**E**) of 7G1 immunostaining in the spinal cord. The threshold image was generated as described in the Material and Methods. The pixels with an optical intensity at or above the threshold are in red. The border of the brain section is outlined with black lines. **F–G:** The photomicrograph

(**F**) and the threshold image (**G**) of FMRP immunostaining in the caudal brainstem at the level of the inferior olive complex (IO). Scale bar: 100 μm (B); 1 mm (G; applies to D–G).

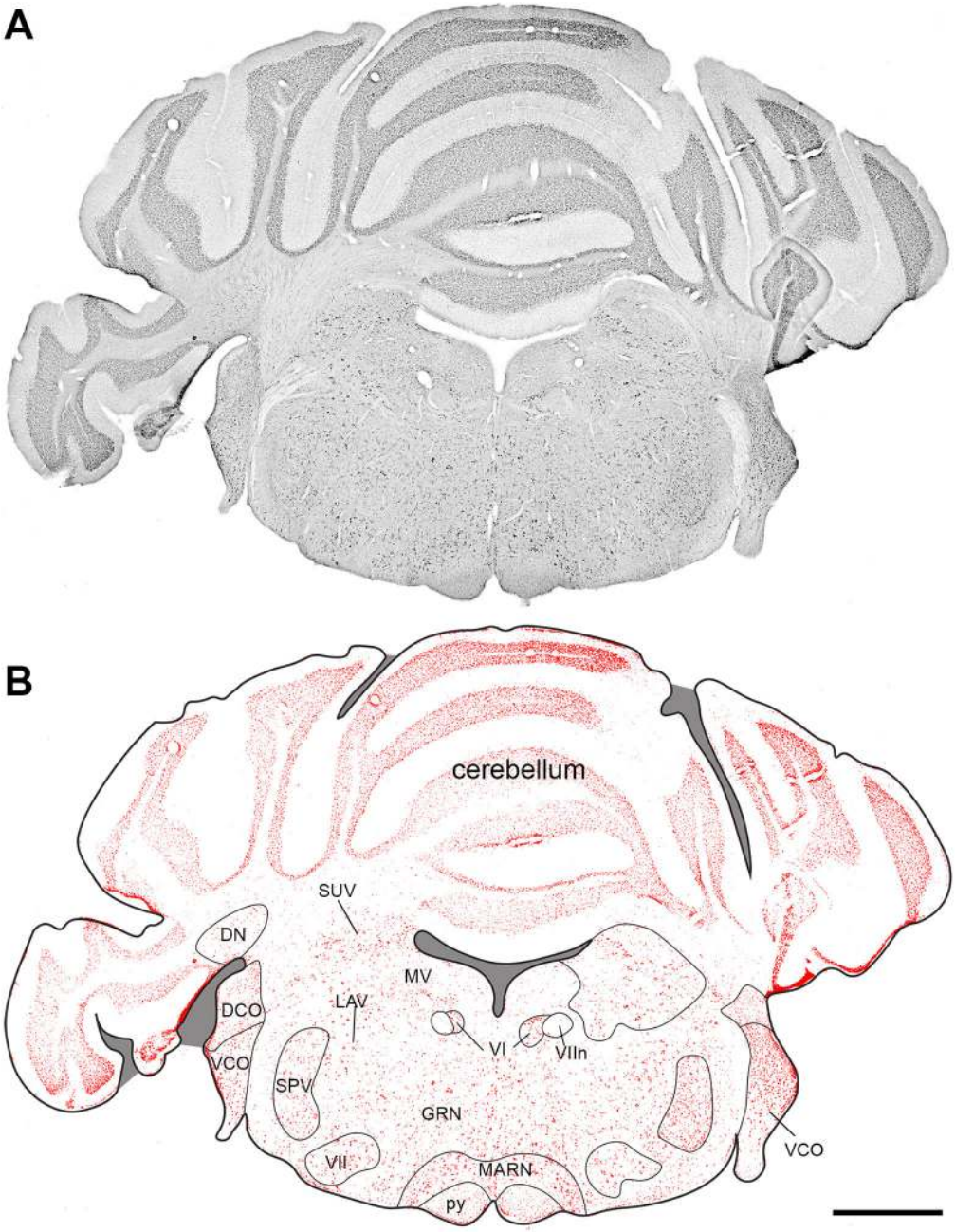

Figure 6.

FMRP (7G1) immunostaining in the coronal plane at the level of the cerebellum and cochlear nuclei. **A,** The photomicrograph. **B,** The threshold image. Grey shades indicate the ventricle and areas without brain tissue. Scale bar: 1 mm.

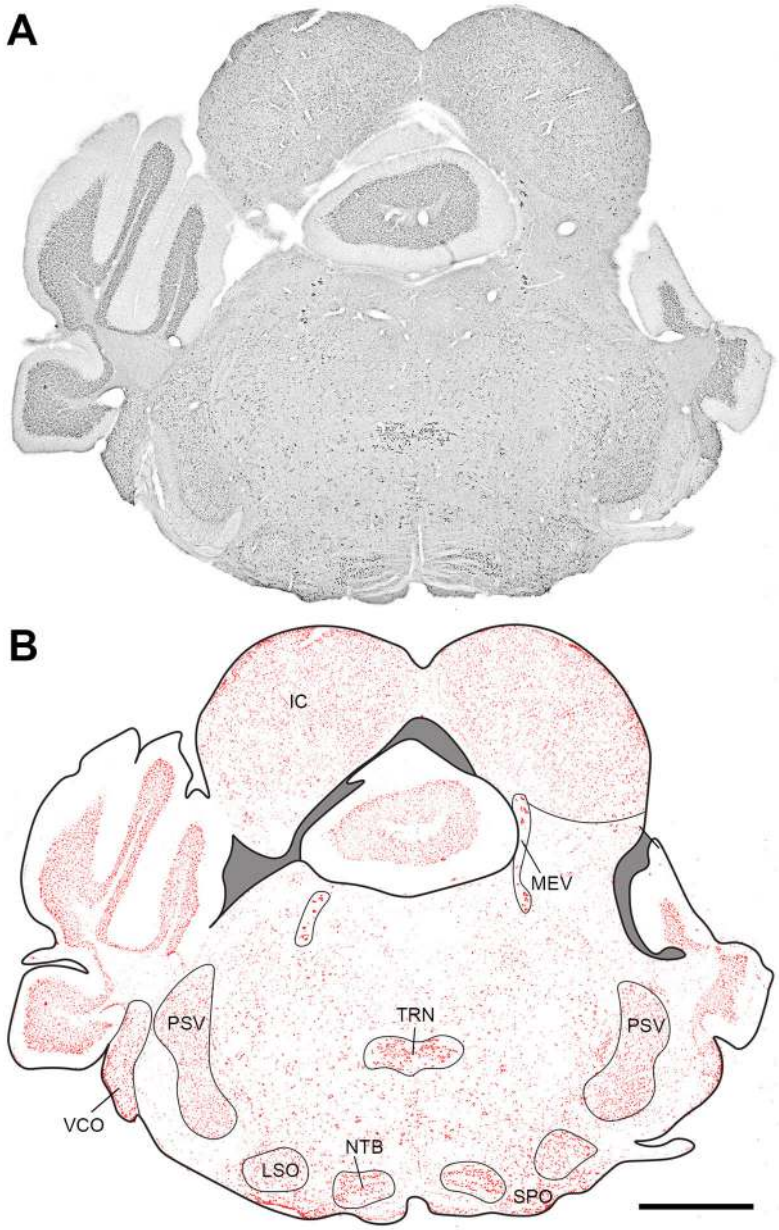

Figure 7.

FMRP (7G1) immunostaining in the coronal plane at the level of the inferior colliculus. **A,** The photomicrograph. **B,** The threshold image. Grey shades indicate the ventricle and areas without brain tissue. Scale bar: 1 mm.

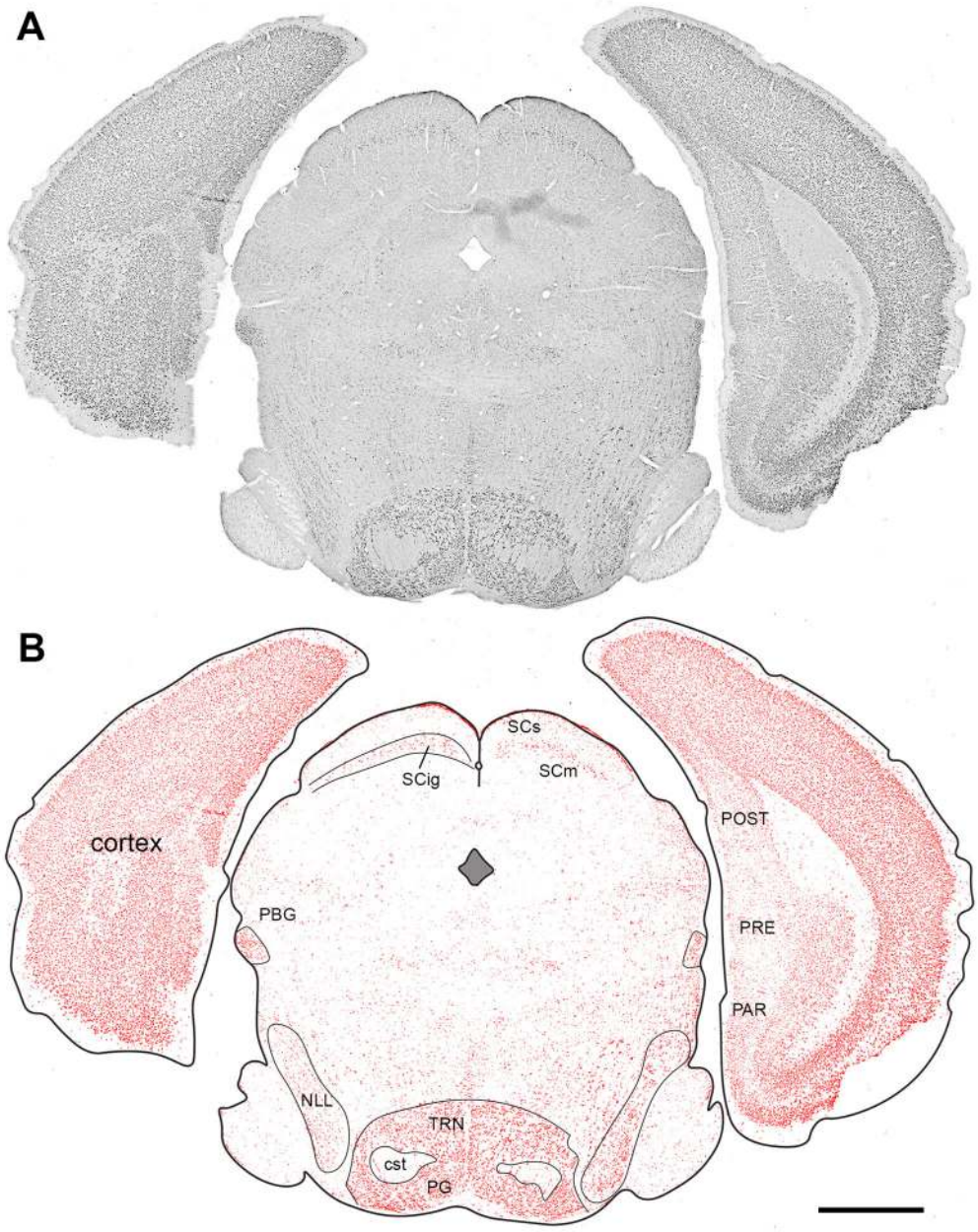

Figure 8.

FMRP (7G1) immunostaining in the coronal plane at the level of the superior colliculus. **A,** The photomicrograph. **B,** The threshold image. Grey shade indicates the ventricle. Scale bar: 1 mm.

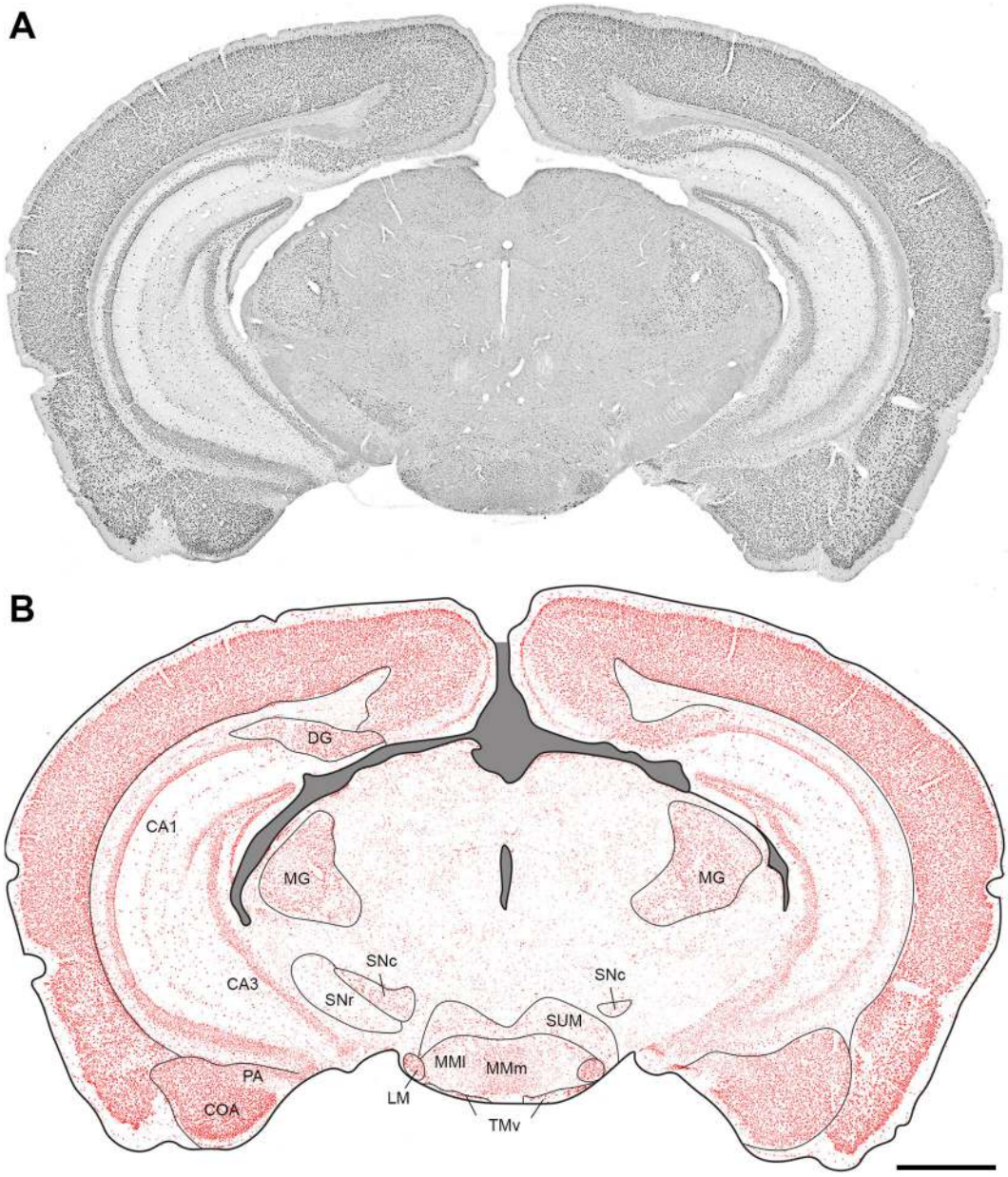

Figure 9.

FMRP (7G1) immunostaining in the coronal plane at the level of the isocortex and caudal thalamus. **A,** The photomicrograph. **B,** The threshold image. Grey shades indicate the ventricle and areas without brain tissue. Scale bar: 1 mm.

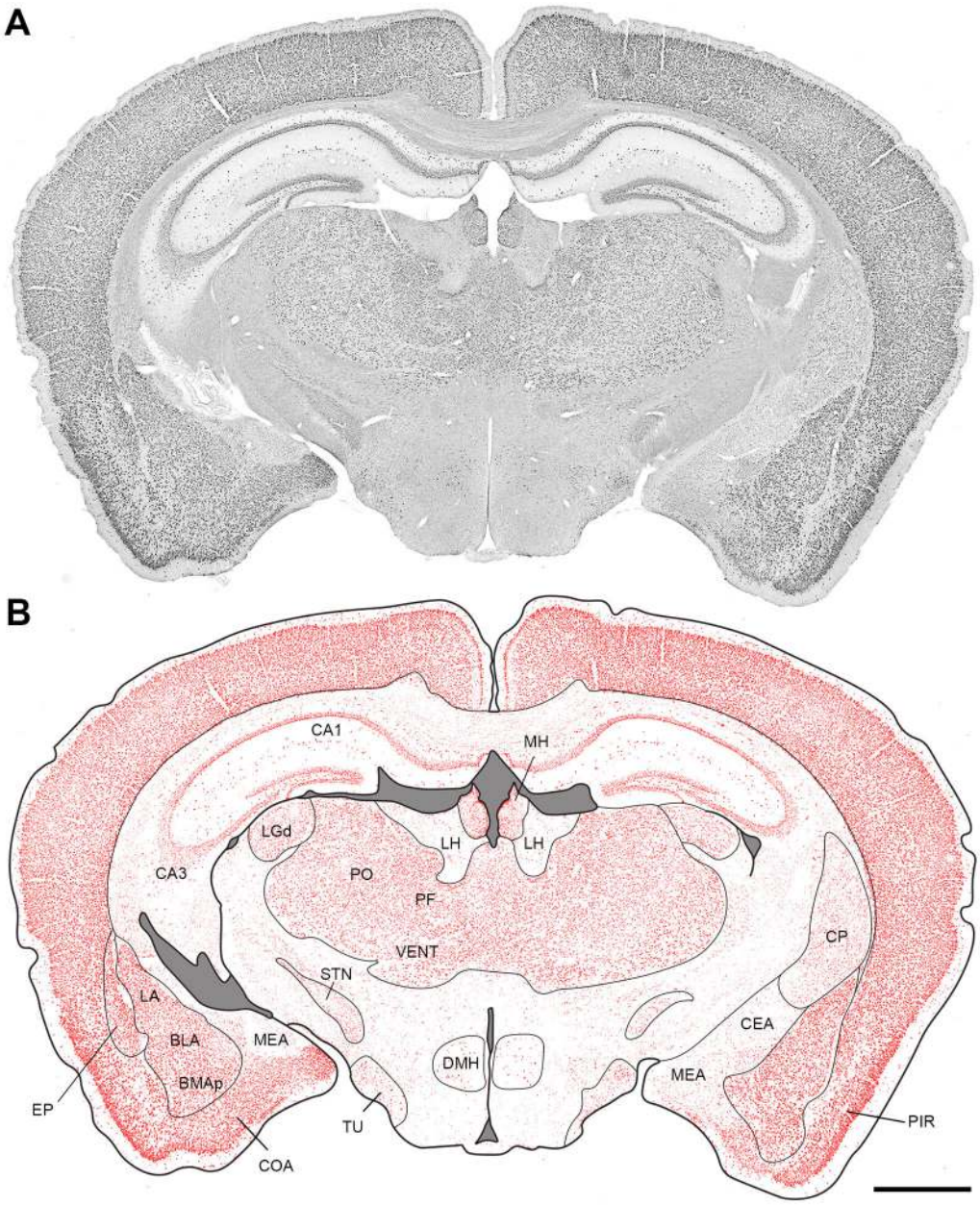

Figure 10.

FMRP (7G1) immunostaining in the coronal plane at the level of the isocortex and middle thalamus. **A,** The photomicrograph. **B,** The threshold image. Grey shades indicate the ventricle and areas without brain tissue. Scale bar: 1 mm.

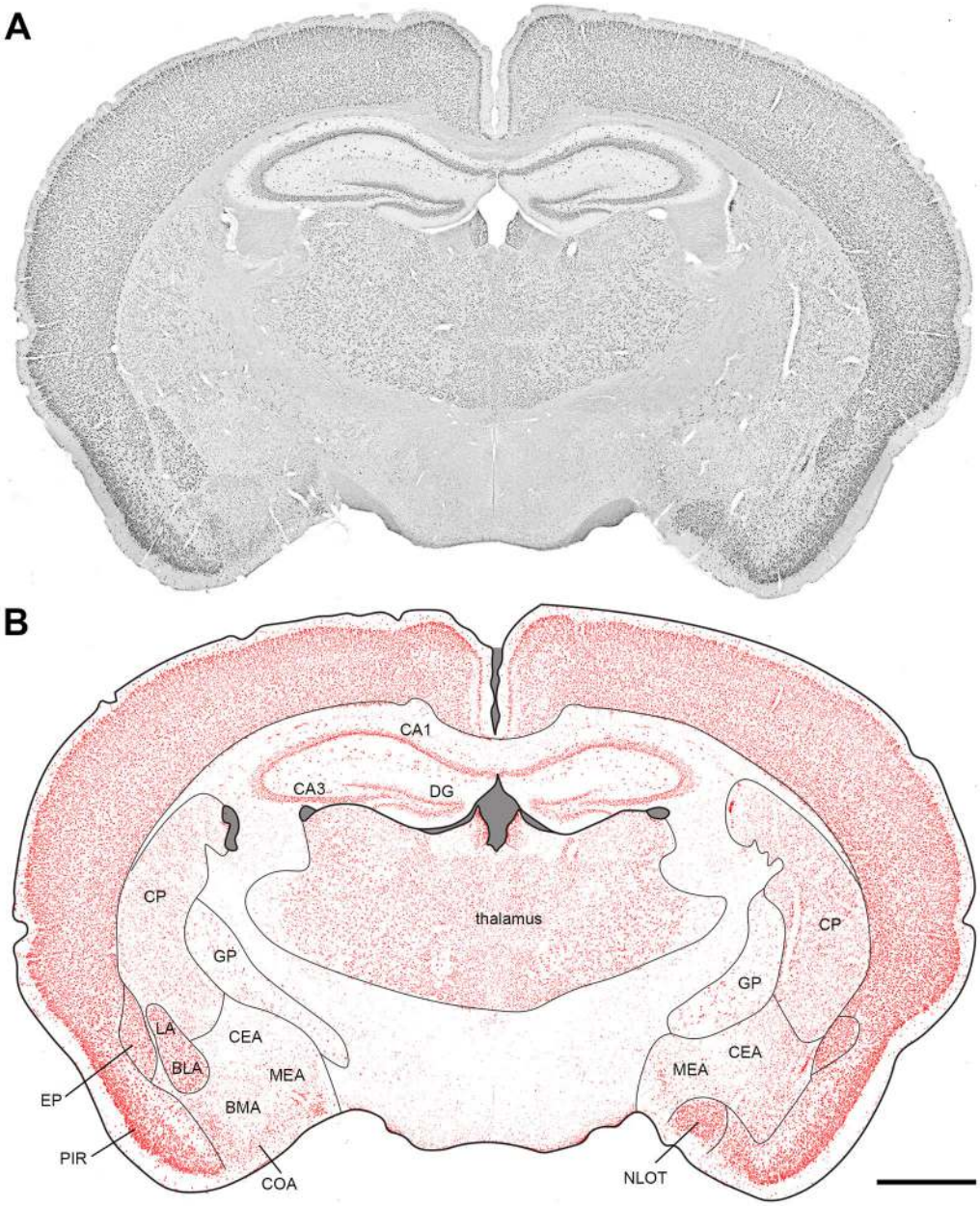

Figure 11.

FMRP (7G1) immunostaining in the coronal plane at the level of the isocortex and rostral thalamus. **A,** The photomicrograph. **B,** The threshold image. Grey shades indicate the ventricle and areas without brain tissue. Scale bar: 1 mm.

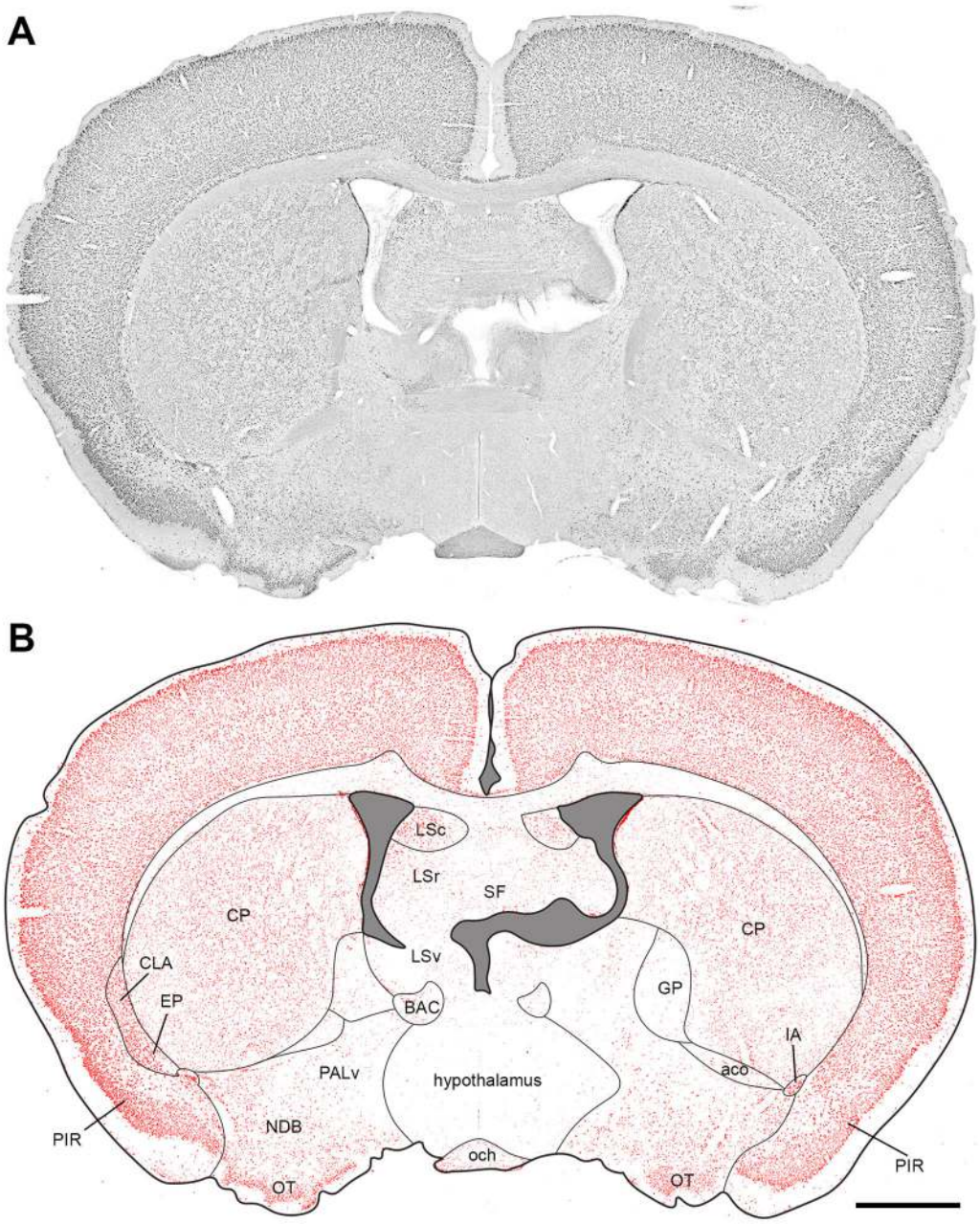

Figure 12.

FMRP (7G1) immunostaining in the coronal plane at the level of the caudal striatum. **A,** The photomicrograph. **B,** The threshold image. Grey shades indicate the ventricle and areas without brain tissue. Scale bar: 1 mm.

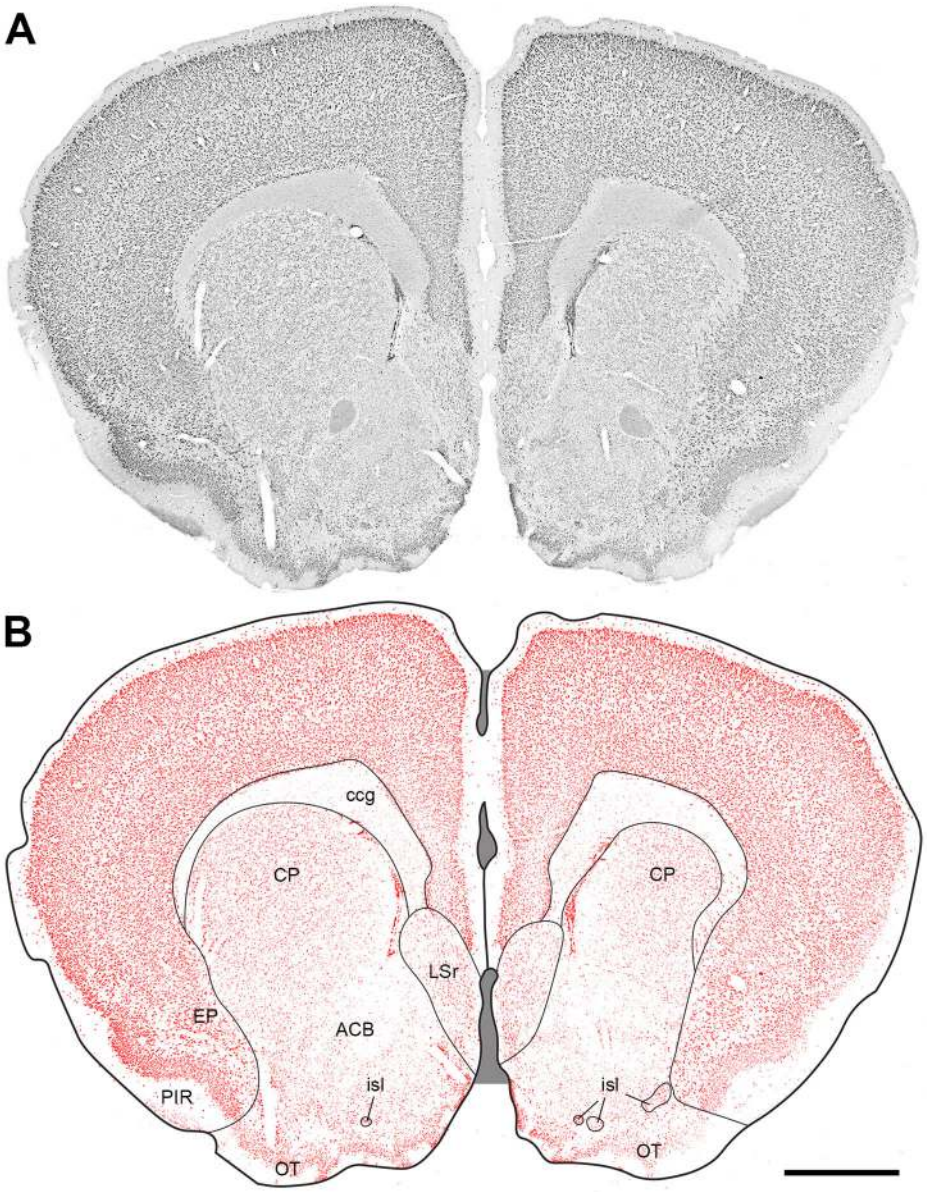

Figure 13.

FMRP (7G1) immunostaining in the coronal plane at the level of the rostral striatum. **A,** The photomicrograph. **B,** The threshold image. Grey shades indicate the ventricle and areas without brain tissue. Scale bar: 1 mm.

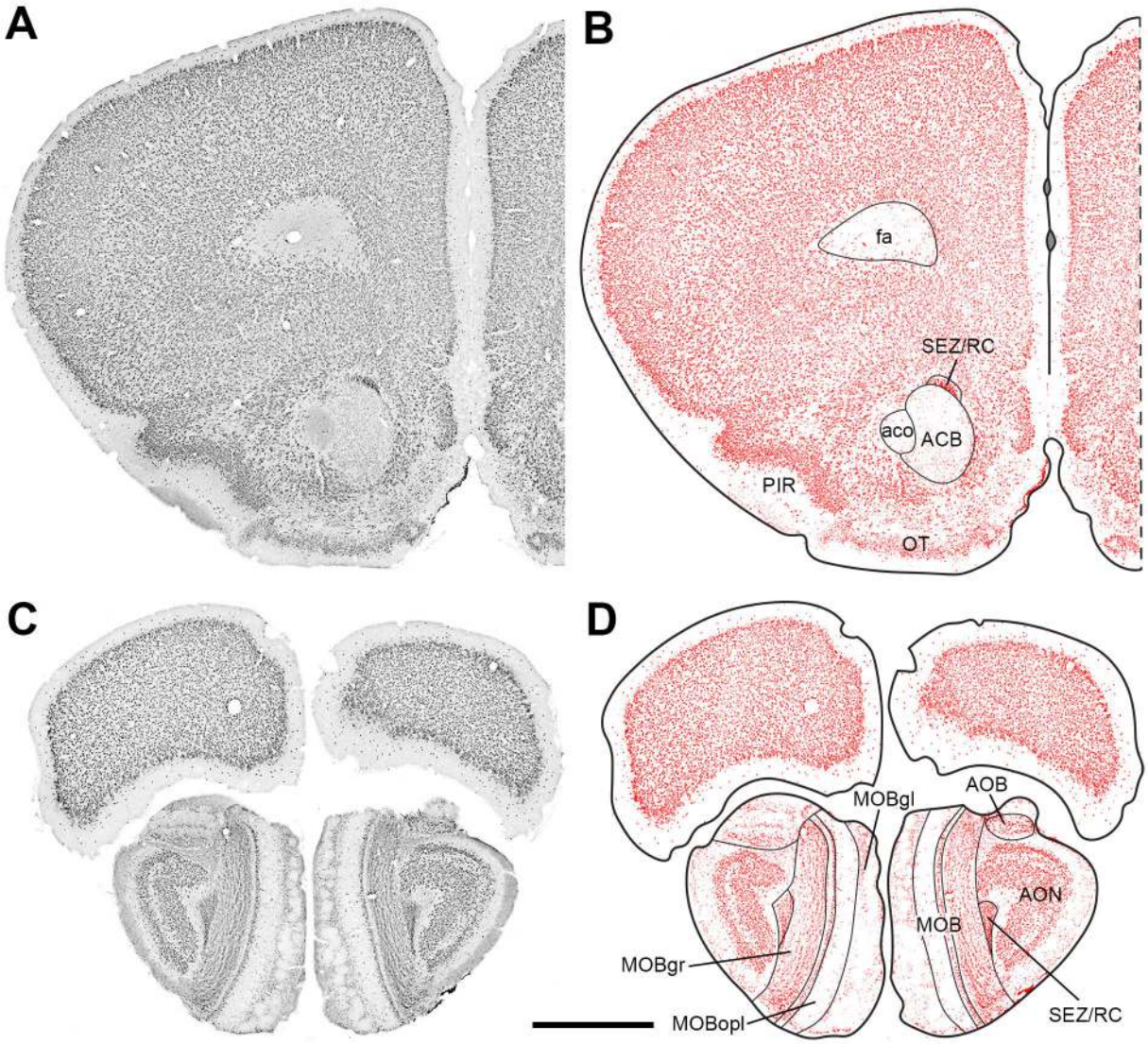

Figure 14.

FMRP (7G1) immunostaining in the coronal plane at the level of the rostral cortex (**A–B**) and olfactory bulb (**C–D**). **A and C,** The photomicrographs. **B and D,** The threshold images. Scale bar: 1 mm.

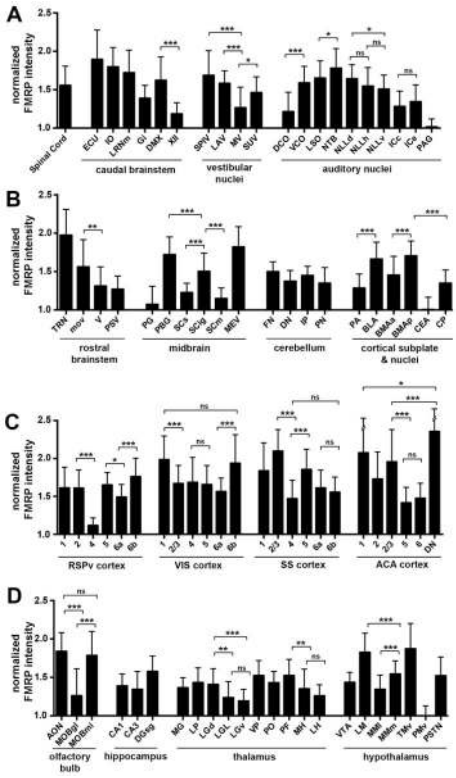

Figure 15.

Cellular quantification of FMRP intensity in selected neuronal cell groups. **A,** The spinal cord and cell groups in the caudal brainstem and vestibular and auditory nuclei. **B,** Cell groups in the rostral brainstem, midbrain, cerebellum, as well as the cortical subplate and nuclei. **C,** Layers of isocortical areas. **D,** Cell groups in the olfactory bulb, hippocampus, thalamus, and hypothalamus. FMRP intensities were normalized as described in the Materials and Methods. Higher intensities indicate higher levels of FMRP staining at the individual cell level. For each cell group, 30 neurons were measured and averaged. Measurements for each cortical area were taken at levels comparable to Figure 24. Error bars are S.D. * indicates $p < 0.01$. ** indicates $p < 0.001$. *** indicates $p < 0.0001$. “ns” indicates not significant.

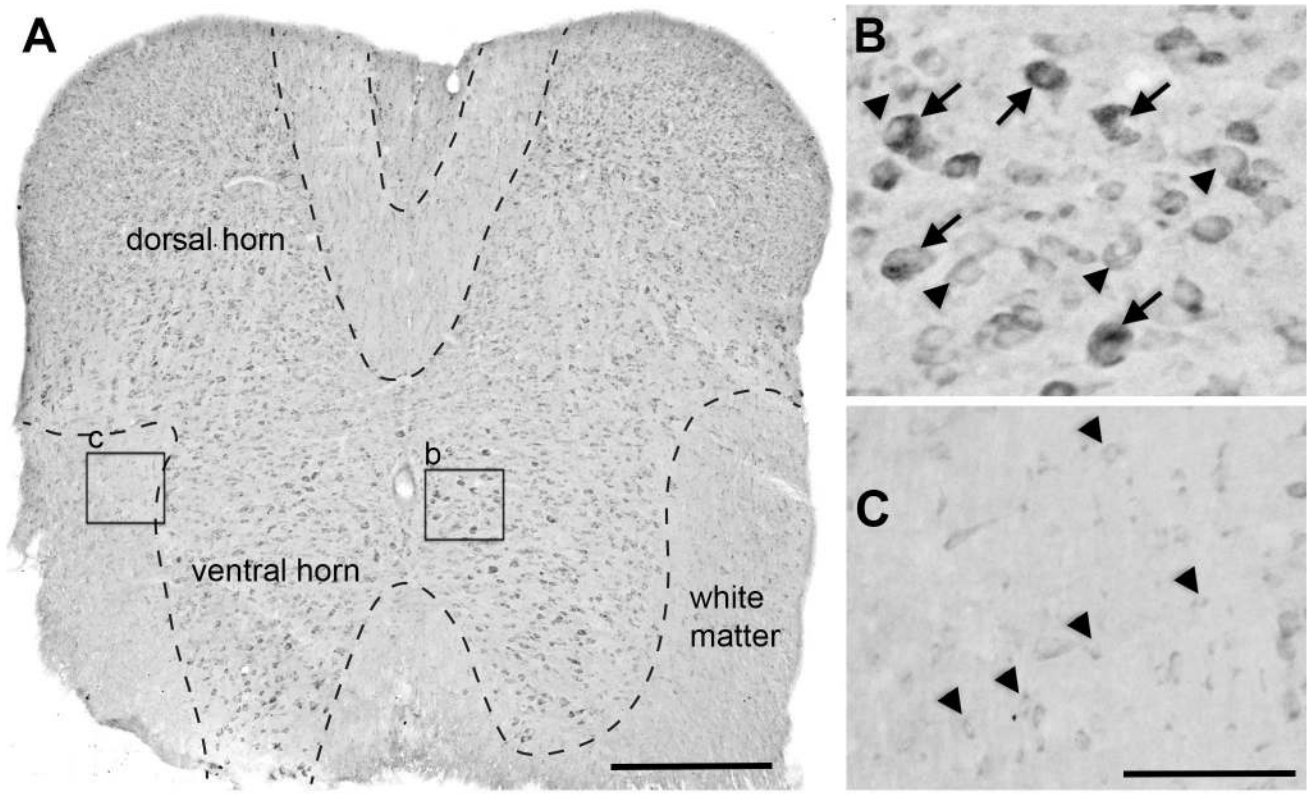

Figure 16.

High-magnification images of FMRP (7G1) immunostaining in the spinal cord. **A,** The spinal cord at the approximate level of C-2 segment. Closer looks of the boxes are displayed in B and C. Dashed lines indicate the borders between the white and grey matters. **B,** The grey matter contains darkly (arrows) and relatively lightly (arrowheads) stained cells. **C,** The white matter contains small immunoreactive cell bodies (arrowheads), presumably glial cells. Scale bar: 500 μm (A), 100 μm (C, applies to B–C).

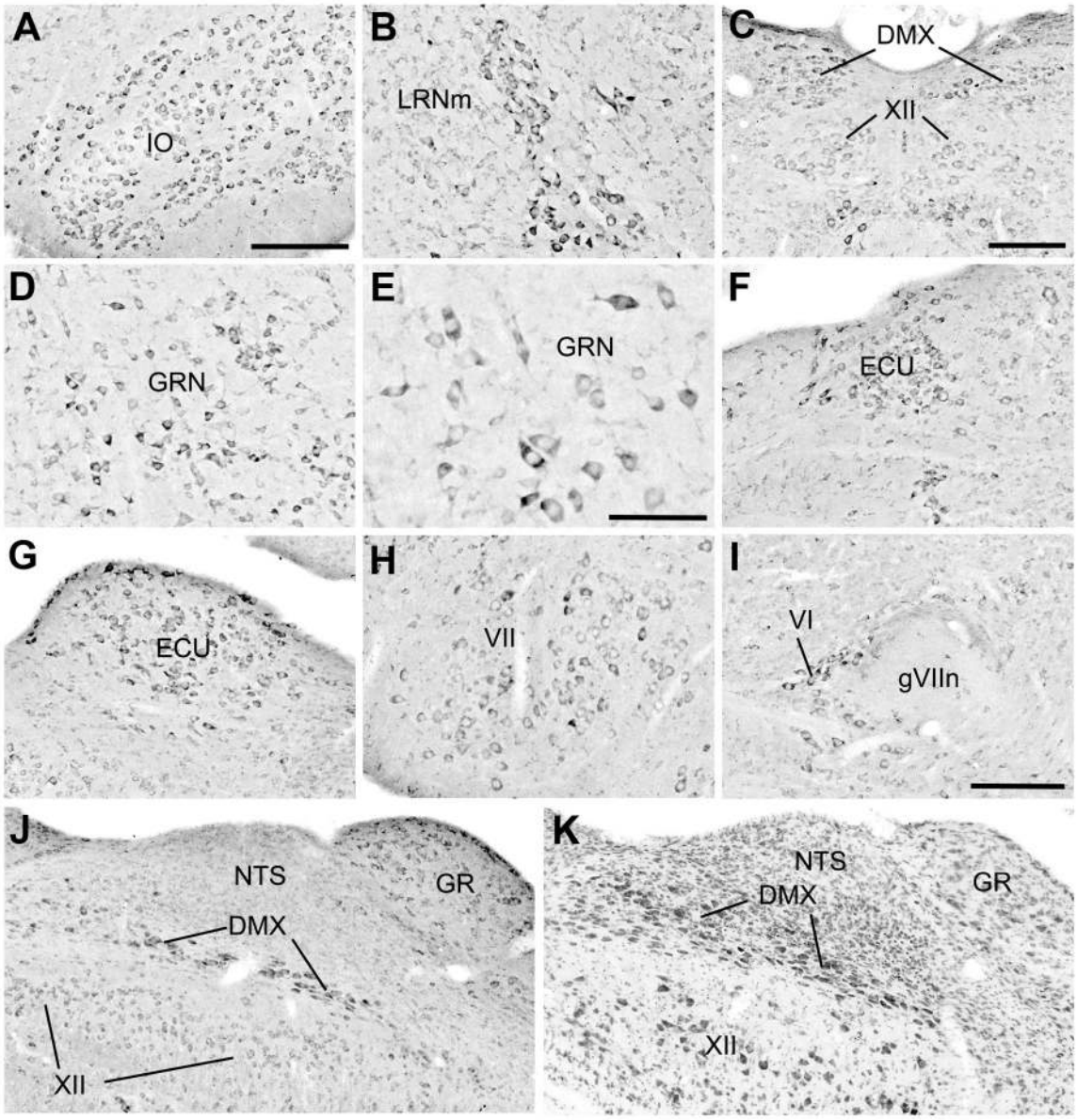

Figure 17.

High-magnification images of FMRP (7G1) immunostaining in the caudal brainstem. **A–B,** High FMRP levels in the inferior olive complex (IO; **A**) and the magnocellular part of the lateral reticular nucleus (LRNm; **B**). **C:** The dorsal motor nucleus of the vagus nerve (DMX) exhibits stronger FMRP staining than the adjacent hypoglossal nucleus (XII). These two nuclei are also illustrated in J and K. **D–E,** The giganticellular reticular nucleus (GRN) contains darkly labeled neurons. E is at a higher magnification than D. **F–G,** The external cuneate nucleus (ECU) is rich in FMRP at both the rostral (**F**) and caudal (**G**) levels. **H–I,** FMRP immunoreactive neurons in the facial motor nucleus (VII; **H**) and the abducens nucleus (VI; **I**). **J–K,** 7G1 immunostaining (**J**) and the Nissl stain (**K**) on the adjacent sections containing DMX and XII. Note the relatively lower level of FMRP in XII as

compared to the DMX. A–I are coronal sections while J–K are sagittal sections. Scale bar: 200 μm (A; applies to A, B, D, F–H, J–K); 200 μm (C, I); 100 μm (E).

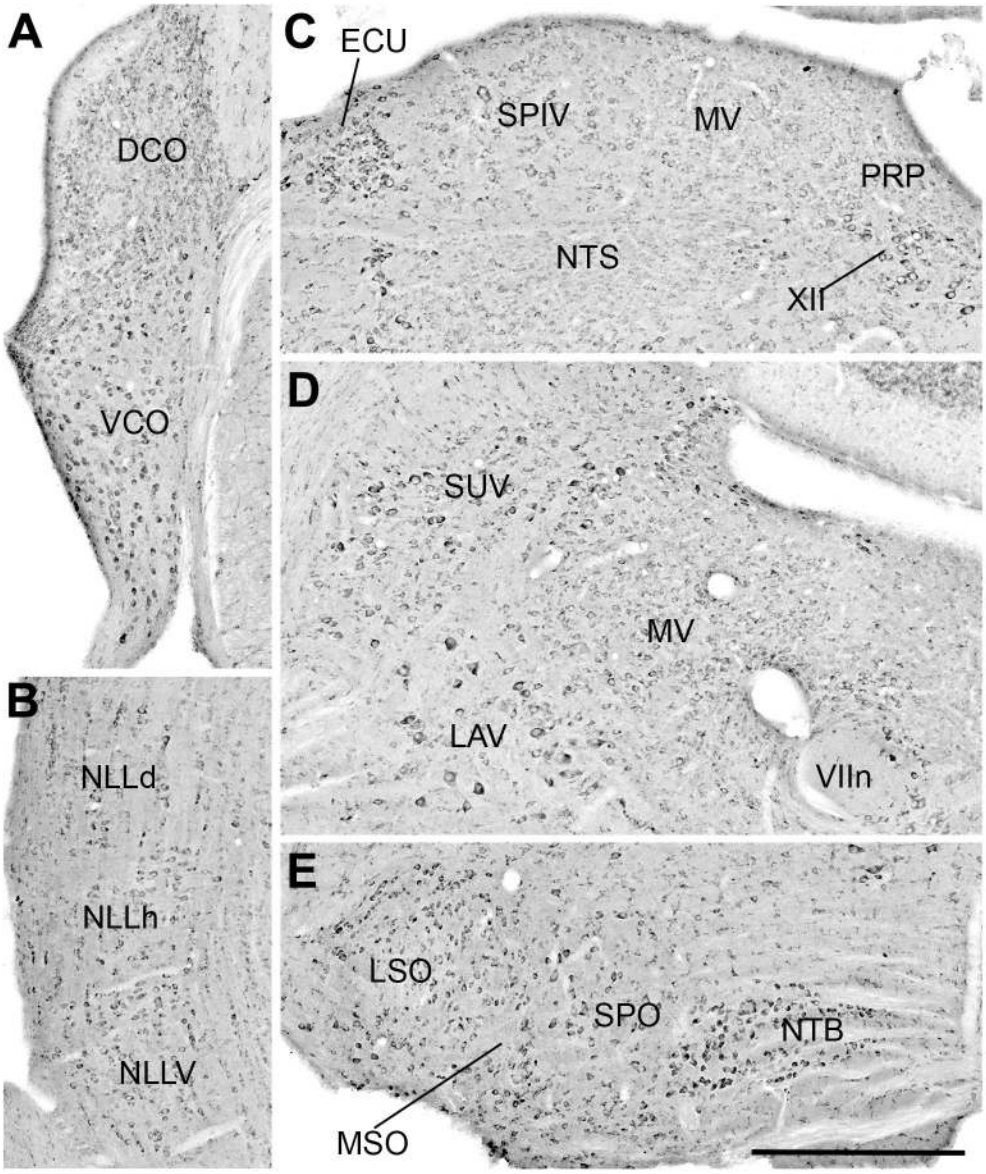

Figure 18.

High-magnification images of FMRP (7G1) immunostaining in the vestibular and auditory brainstem nuclei. **A,** FMRP staining in the dorsal and ventral cochlear nuclei (DCO and VCO). **B,** FMRP staining in the three subnuclei of the nucleus of the lateral lemniscus (NLLd, NLLh, and NLLV). **C–D,** FMRP staining in the medial, spinal, lateral, and superior portions of the vestibular nucleus (MV, SPIV, LAV, and SUV). D was taken from a section more rostral than C. **E,** FMRP staining in the superior olive complex and the nucleus of the trapezoid body (NTB). Scale bar: 500 μm.

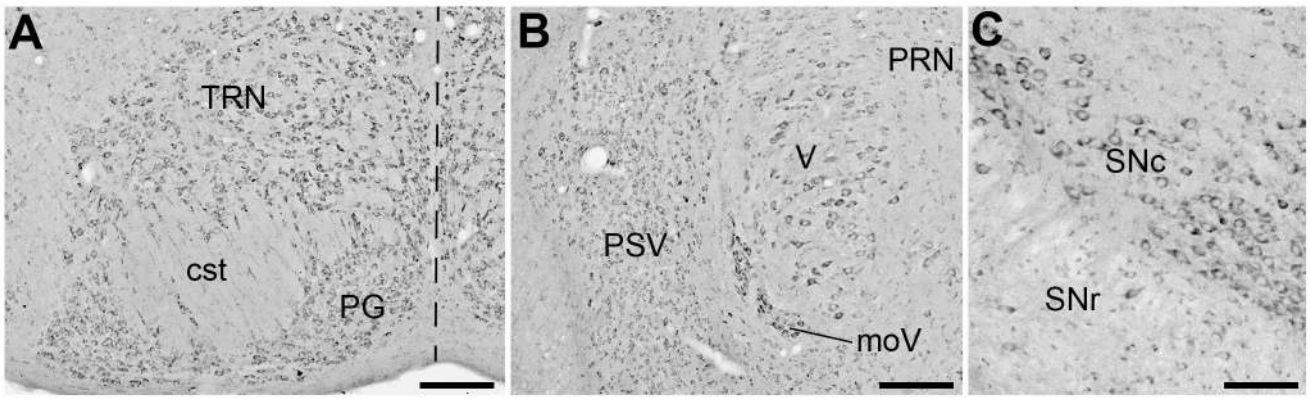

Figure 19.

High-magnification images of FMRP (7G1) immunostaining in the rostral brainstem. **A,** Intense FMRP staining in the tegmental reticular nucleus (TRN) and the pontine gray (PG). Dashed line indicates the midline. **B,** FMRP staining in the principal sensory nucleus of the trigeminal (PSV) and the motor nucleus of the trigeminal (V). Note particularly high FMRP levels in neurons embedded in the motor root of the trigeminal nerve (moV). **C,** FMRP immunoreactive neurons in the compact pact of the substantia nigra (SNc). Scale bar: 200 μm (A, B); 100 μm (C).

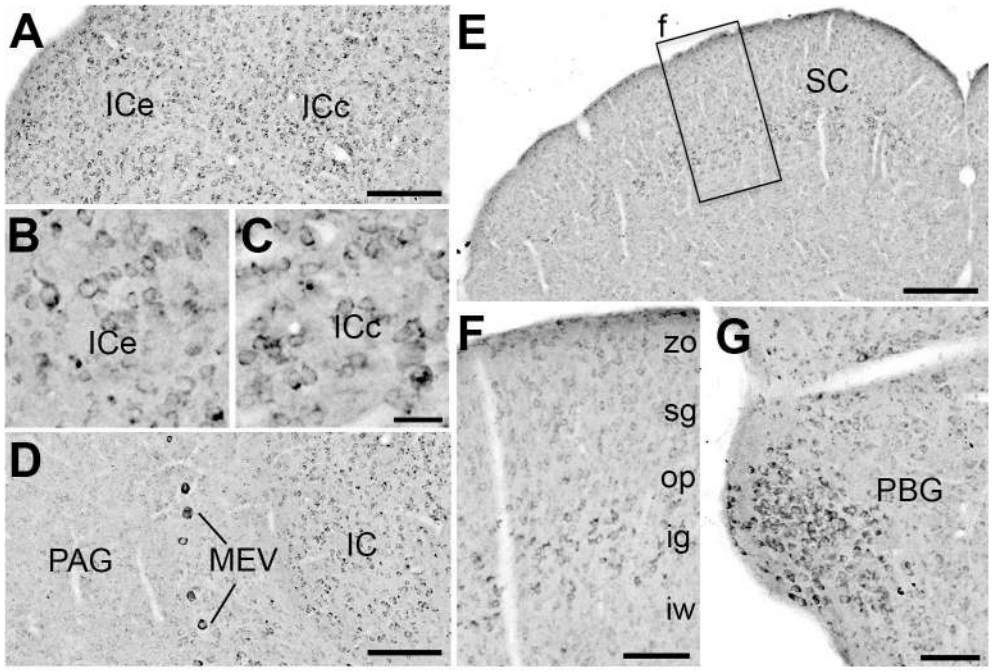

Figure 20.

High-magnification images of FMRP (7G1) immunostaining in midbrain cell groups. **A–C,** FMRP immunoreactivity in the external and central nuclei of the inferior colliculus (ICe and ICc). B and C are at a higher magnification than A. **D,** FMRP staining is weak in the adjacent periaqueductal gray (PAG). Note darkly labeled neurons in the midbrain trigeminal nucleus (MEV). **E–F,** Intense FMRP staining in the intermediate gray layer (ig), but not other layers, of the superior colliculus (SC). F is a closer look of the box in E. **G,** Neurons in the parabigeminal nucleus are darkly labeled for FMRP immunocytochemistry. Scale bar: 250 μm (A, D, E); 50 μm (B; applies to B, C); 100 μm (F, G).

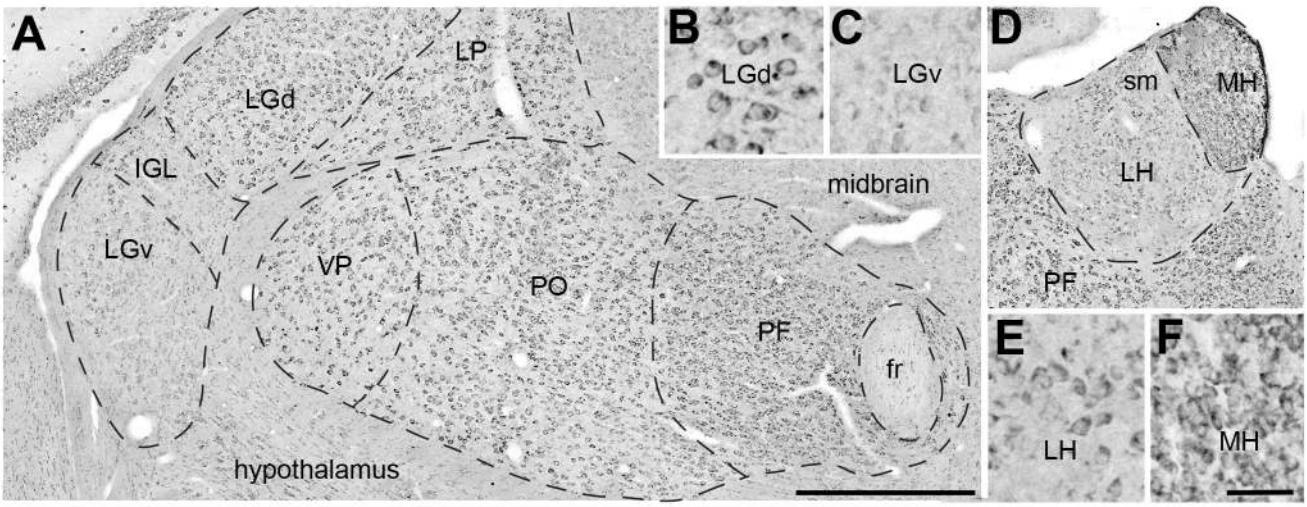

Figure 21.

High-magnification images of FMRP (7G1) immunostaining in the thalamus. **A,** Strong FMRP staining in most thalamic cell groups but not the ventral portion of the lateral geniculate complex (LGv) and the intergeniculate leaflet (IGL). **B–C,** Closer looks of the neurons in the dorsal portion of the LG (LGd; **B**) and LGv (**C**). **D,** FMRP staining appears stronger in the medial habenula (MH) than the lateral habenula (LH). **E–F,** Closer looks of the neurons in the LH (**E**) and MH (**F**). Note FMRP intensity at the individual cell level is comparable between these two cell groups, although MH has a higher cell density. Dashed lines outline the approximate location of different cell groups. Scale bar: 500 μm (A; applies to A, D); 50 μm (F; applies to B, C, E, F).

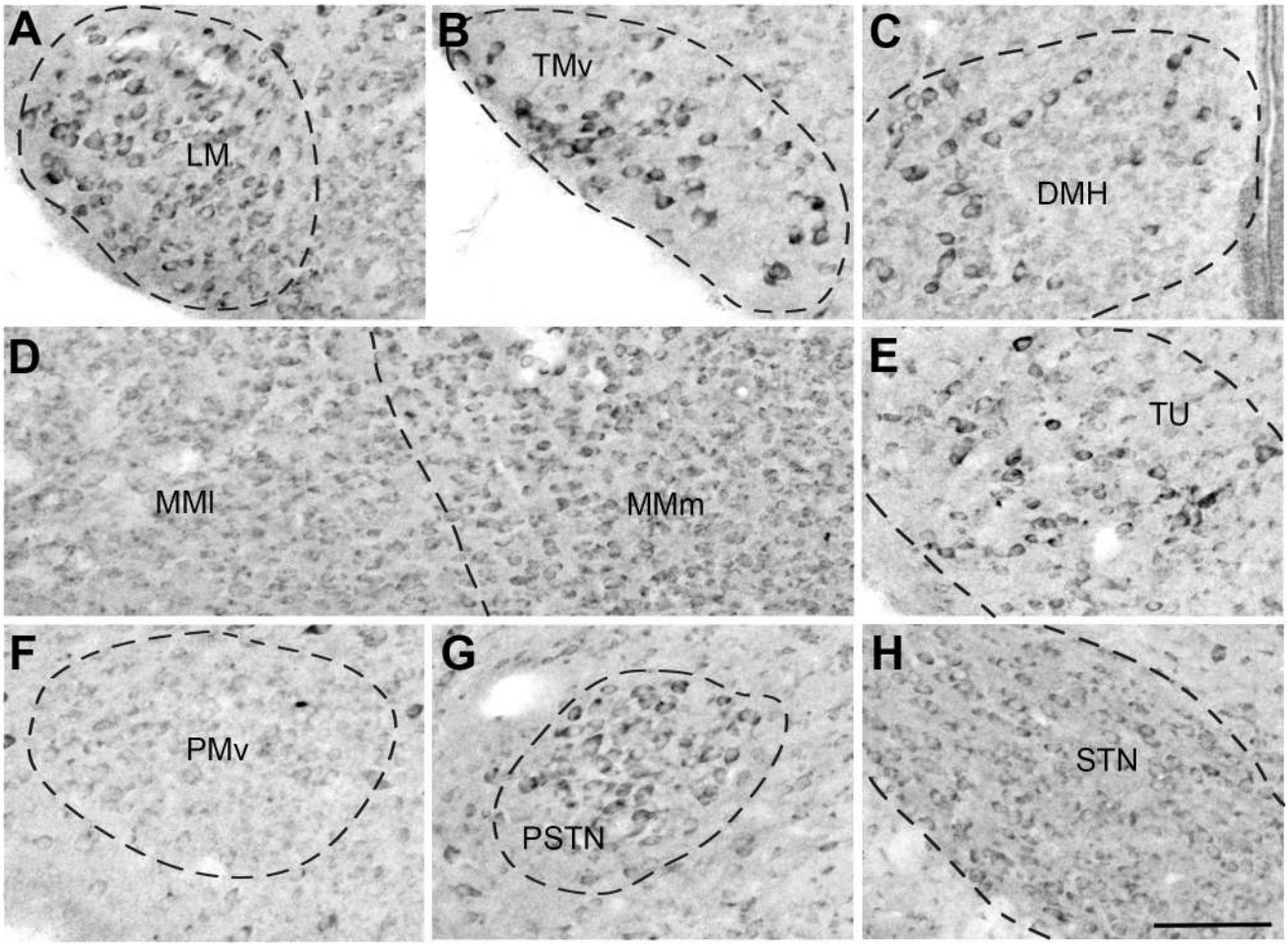

Figure 22.

High-magnification images of FMRP (7G1) immunostaining in the hypothalamus. FMRP staining is strong in the lateral mammillary nucleus (LM; **A**), the ventral part of the tuberomammillary nucleus (TMv; **B**), the dorsomedial nucleus of the hypothalamus (DMH; **C**), the medial part of the medial mammillary nucleus (MMm; **D**), the tuberal nucleus (TU; **E**), the parasubthalamic nucleus (PSTN; **G**), and the subthalamic nucleus (STN; **H**). In contrast, FMRP staining is weak in the ventral premammillary nucleus (PMv; **F**). Note that FMRP staining is weaker in the lateral part of the medial mammillary nucleus (MMl) than in the MMm (**D**). Dashed lines outline the approximate location of different cell groups. Scale bar: 100 μm.

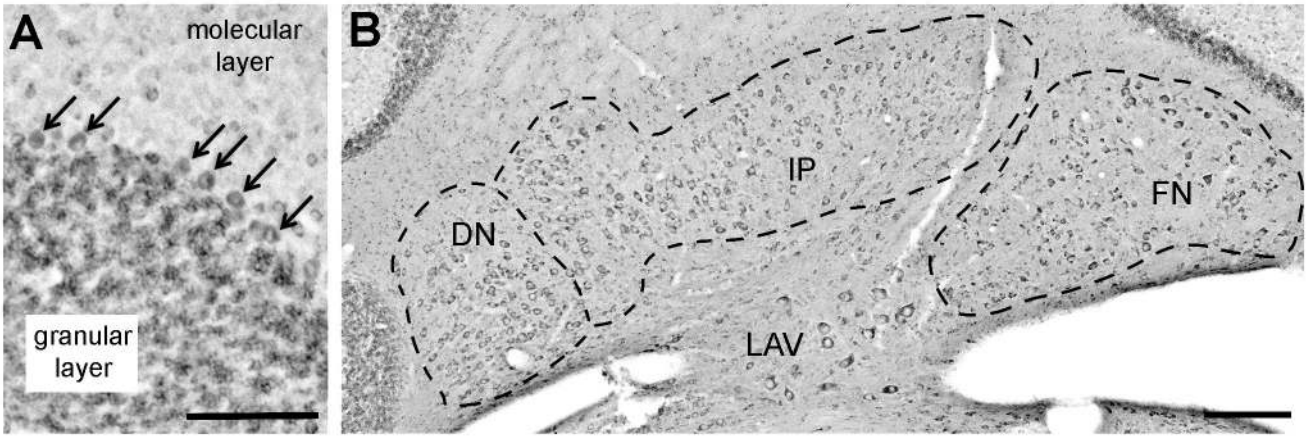

Figure 23.

High-magnification images of FMRP (7G1) immunostaining in the cerebellum. **A,** Strong FMRP staining in purkinje neurons (arrows) and granular layer but not in the molecular layer. **B,** FMRP staining in the three cerebellar nuclei. Dashed lines outline the approximate location of these nuclei. Scale bar: 100 μm (A); 200 μm (B).

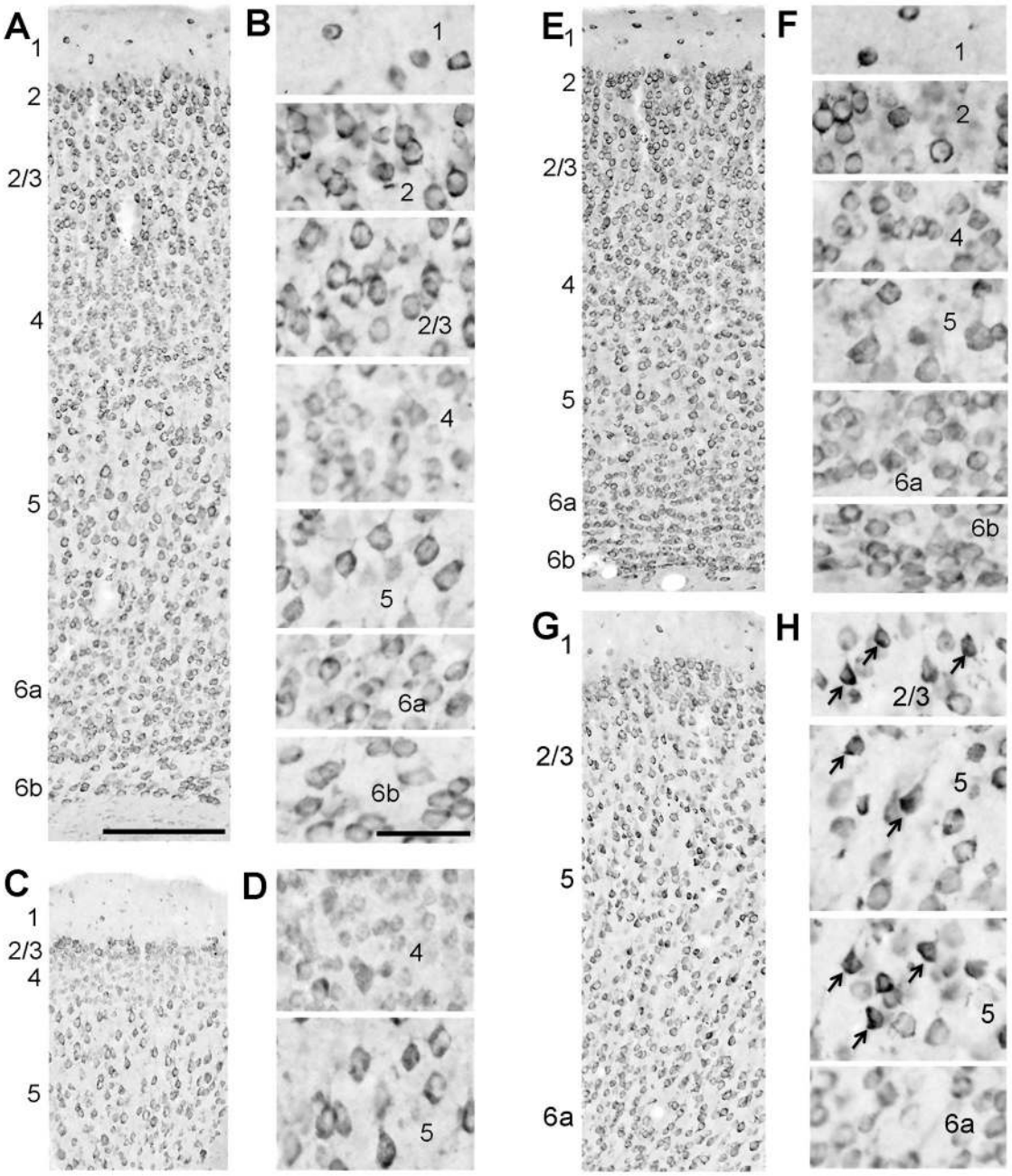

Figure 24.

High-magnification images of FMRP (7G1) immunostaining in the isocortex. **A–B,** The primary somatosensory area taken from the level comparable to Figure 12. B are closer looks of individual layers in A. **C–D,** The ventral part of retrosplenial area taken from the level comparable to Figure 9. D are closer looks of individual layers in C. **E–F,** The primary visual area taken from the level comparable to Figure 9. F are closer looks of individual layers in E. **G–H,** The anterior cingulate area taken from the level comparable to Figure 12. H are closer looks of individual layers in G. Note that neurons in the layer 4 are more lightly stained than other layers in the somatosensory (A–B) and retrosplenial (C–D), but not in the

visual (E–F), areas. Neurons in the layers 2–3 exhibit stronger staining than other layers in the somatosensory (A–B) and visual (E–F) areas. Arrowheads in H indicate the neurons with uniquely strong staining. Scale bar: 200 μm (A; Applies to A, C, E, G); 50 μm (B; applies to B, D, F, H).

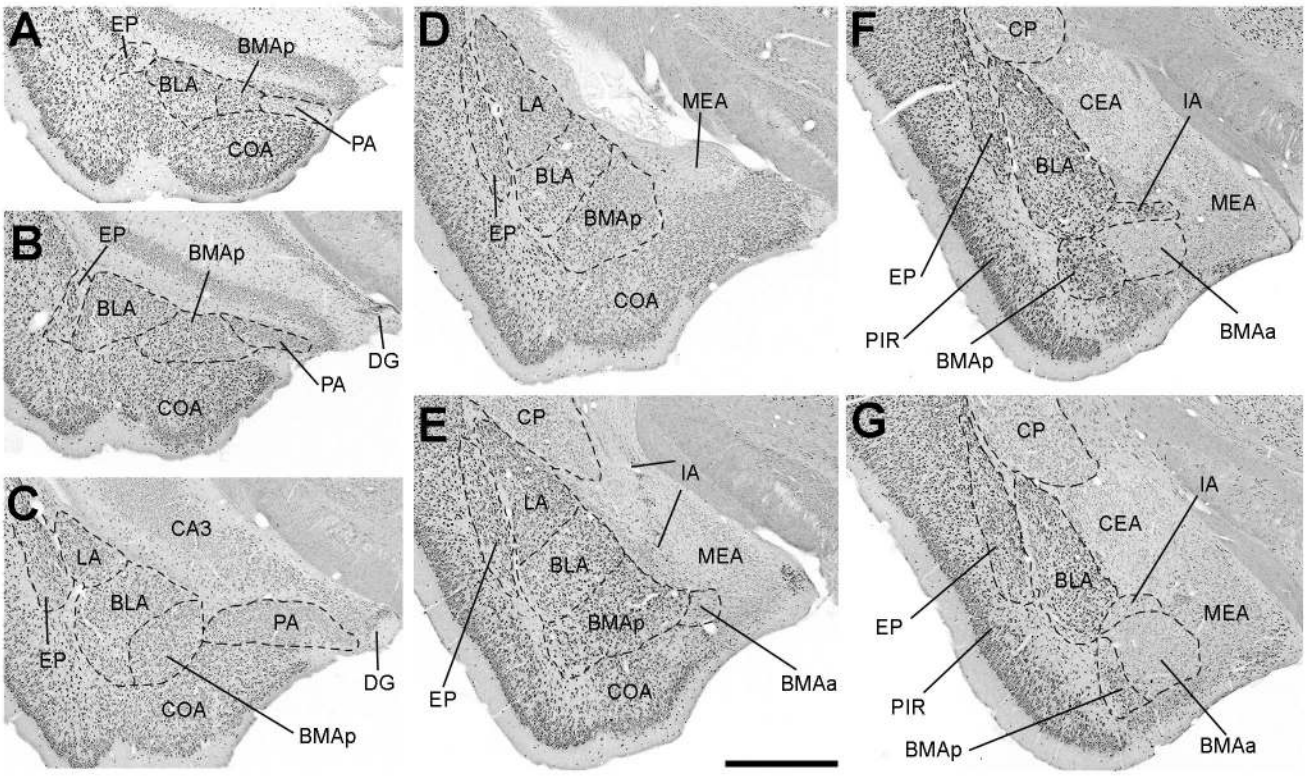

Figure 25.

High-magnification images of FMRP (7G1) immunostaining in the cortical subplate and striatum. **A–G,** Serials images throughout the cortical subplate from caudal (A) to rostral (G). Dashed lines outline the approximate boundaries of a number of nuclei. Scale bar: 500 μm.

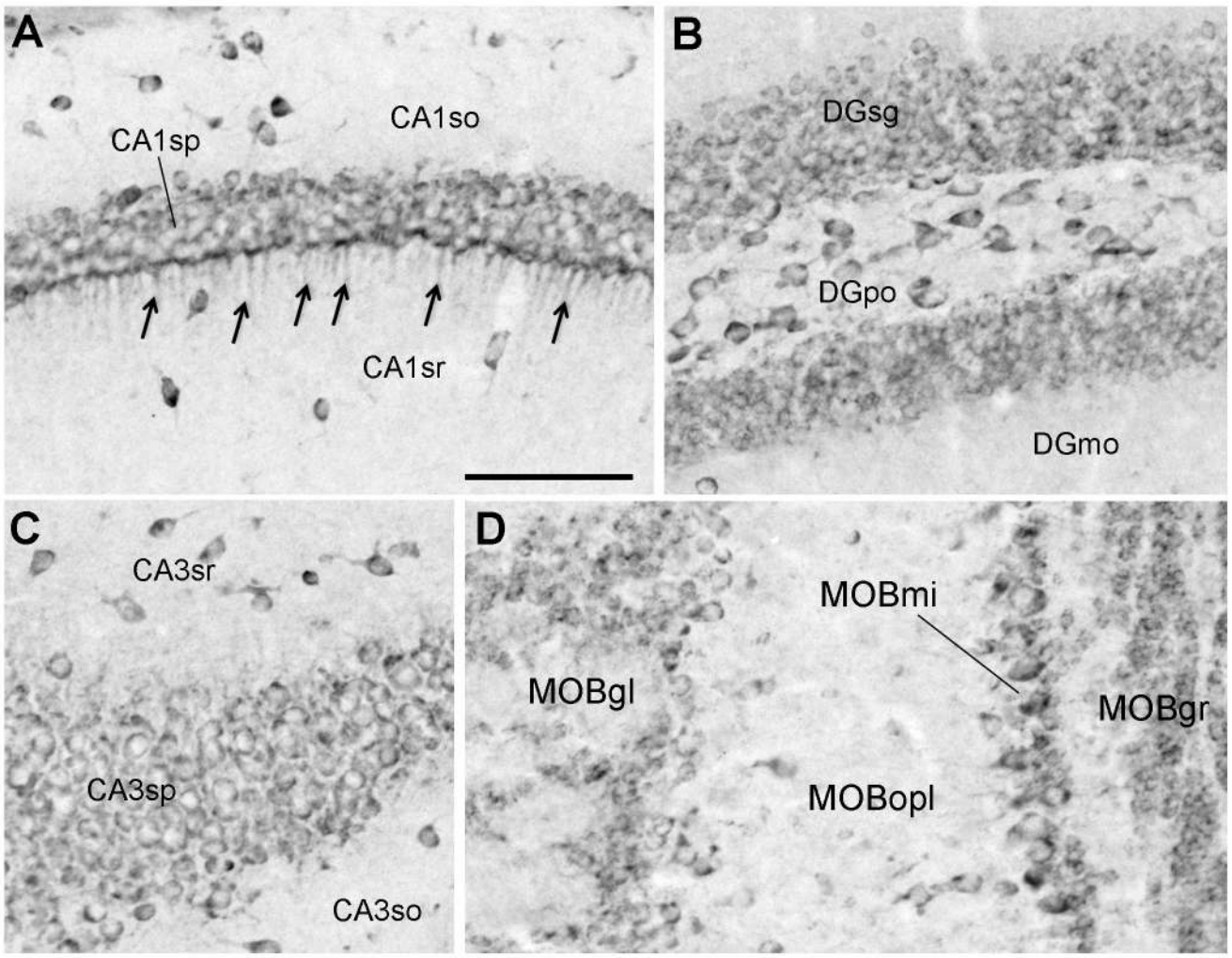

Figure 26.

High-magnification images of FMRP (7G1) immunostaining in the hippocampus and the main olfactory bulb (MOB). **A,** FMRP staining in the hippocampus CA1. Arrows indicate stained dendrites of the pyramidal neurons. **B,** FMRP staining in the dentate gyrus (DG). **C,** FMRP staining in the hippocampus CA3. **D,** FMRP staining in the MOB. Scale bar: 100 μm.

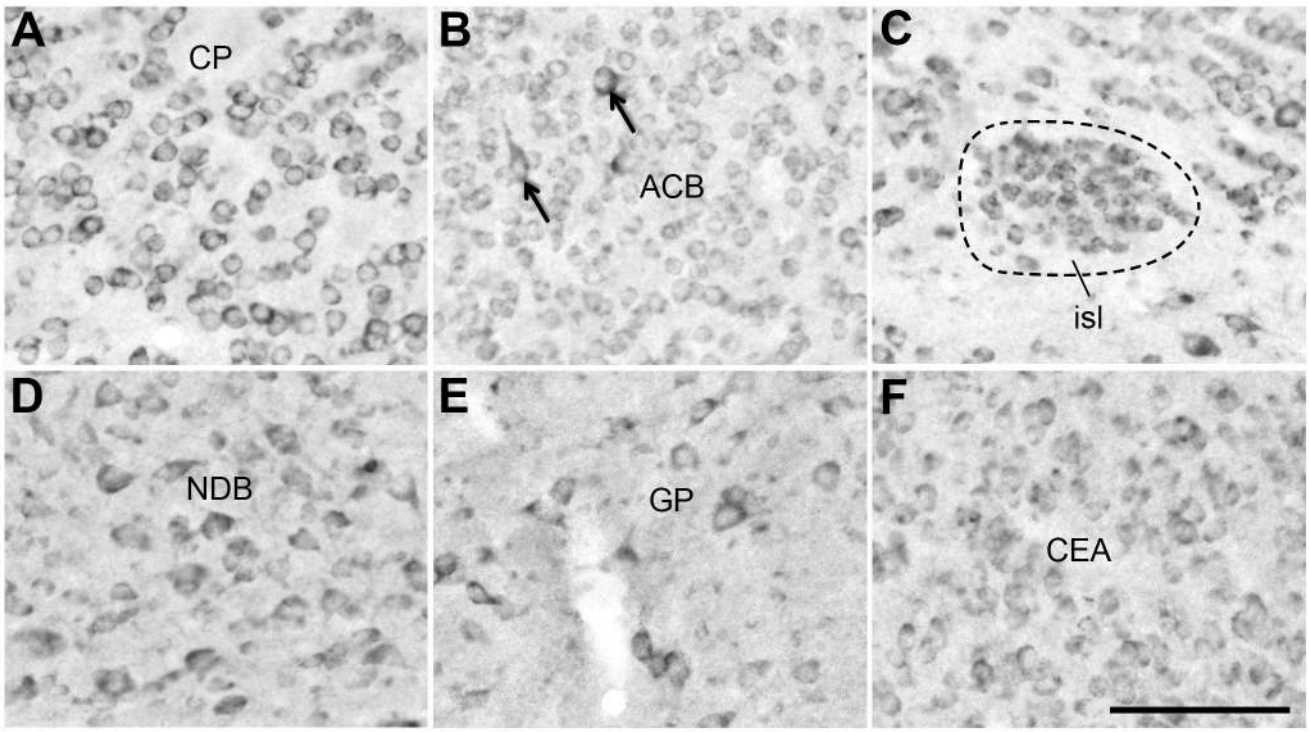

Figure 27.

High-magnification images of FMRP (7G1) immunostaining in the striatum and pallidum. FMRP staining is stronger in the caudoputamen (CP; **A**), the islands of Calleja (isl; **C**), the diagonal band nucleus (NDB; **D**), and the globus pallidus (GP; **E**), than in the nucleus accumbens (ACB; **B**) and the central amygdalar nuclei (CEA; **F**). Arrows in B indicate two more darkly labeled neurons in ACB. Dashed line in C outlines the boundary of one island of Calleja. Scale bar: 100 μm.

Table 1

Primary antibodies used for immunocytochemistry (ICC) and Western blots (WB).

	Antigen	Host, monoclonal or polyclonal, dilution	Manufacturer, catalog number
7G1	amino acid 354-368 (KHLDTKENTHFSQPN) of mouse FMRP-6X-his fusion protein	mouse, monoclonal, 1:500 (ICC); 1:500 (WB)	Developmental Studies Hybridoma Bank (DSHB) at the University of Iowa (Iowa City, IA)
2F5	amino acid 1-204 (N-terminus) of human FMRP-6X-His-tagged fusion protein	mouse, monoclonal, 1:500 (ICC); 1:775 (WB)	DSHB (Iowa City, IA)
β-actin	slightly modified β-cytoplasmic actin N-terminal peptide, G, conjugated to KLH	mouse, monoclonal, 1:5000 (WB)	Sigma, A5316

J Comp Neurol. Author manuscript; available in PMC 2017 August 16.

Table 2

FMRP-rich neuronal cell groups in the mouse brain.

Neuronal cell groups	Neuronal cell groups	Neuronal cell groups
Spinal Cord	**Cerebellum**	**Cerebral Cortex**
Grey matter	Dentate nucleus (DN)	Isocortex – all areas
Brainstem	Fastigial nucleus (FN)	Basolateral amygdalar nucleus (BLA)
Abducens nucleus (VI)	Interposed nucleus (IP)	Basomedial amygdalar nucleus, posterior part (BMAp)
Dorsal motor nucleus of the vagus nerve (DMX)	Granular cells	Claustrum (CLA)
External cuneate nucleus (ECU)	Purkinje neurons	Cortical amygdalar area (COA)
Facial motor nucleus (VII)	**Midbrain**	Endopiriform nucleus (EP)
Gigantocellular reticular nucleus (GRN)	Inferior colliculus (IC)	Lateral amygdalar nucleus (LA)
Gracile nucleus (GR)	Midbrain trigeminal nucleus (MEV)	**Cerebral Nuclei**
Inferior olivary complex (IO)	Parabigeminal nucleus (PBG)	Caudoputamen (CP)
Lateral reticular nucleus, magnocellular part (LRNm)	Red nucleus (RN)	Diagonal band nucleus (NDB)
Motor nucleus of the trigeminal (V)	Substantia nigra, compact part (SNc)	Globus pallidus (GP)
motor root of the trigeminal nerve (moV)	Superior colliculus, intermediate gray layer (SCig)	Intercalated amygdalar nucleus (IA)
Nucleus of the lateral lemniscus (NLL)	**Thalamus**	Islands of Calleja (isl)
Nucleus of the trapezoid body (NTB)	Lateral geniculate complex, dorsal part (LGd)	Medial amygdalar nucleus, posteroventral part (MEApv)
Nucleus raphe obscurus (RO)	Lateral habenula (LH)	Olfactory tubercle (OT)
Nucleus raphe pallidus (RPA)	Lateral posterior nucleus of the thalamus (LP)	**Hippocampus**
Pontine gray (PG)	Medial geniculate complex (MG)	Dentate gyrus (DG)
Principal sensory nucleus of the trigeminal (PSV)	Medial habenula (MH)	Field CA1 (CA1)
Spinal nucleus of the trigeminal (SPV)	Parafascicular nucleus (PF)	Field CA2 (CA2)
Superior olivary complex (SOC)	Posterior complex of the thalamus (PO)	Field CA3 (CA3)
Lateral superior olive (LSO) *	Ventral group of the dorsal thalamus (VENT)	**Olfactory**
Medial superior olive (MSO) *	Ventral posterior complex of the thalamus (VP)	Accessory olfactory bulb (AOB)
Superior paraolivary nucleus (SPO) *	**Hypothalamus**	Anterior olfactory nucleus (AON)
Tegmental reticular nucleus (TRN)	Dorsomedial nucleus of the hypothalamus (DMH)	Main olfactory bulb (MOB)
Ventral cochlear nucleus (VCO)	Lateral mammillary nucleus (LM)	glomerular layer (MOBgl)
Vestibular nuclei (VNC)	Medial mammillary nucleus, medial part (MMm) *	granule layer (MOBgr)
Lateral vestibular nucleus (LAV)	Parasubthalamic nucleus (PSTN)	mitral layer (MOBmi)
Spinal vestibular nucleus (SPIV)	Subthalamic nucleus (STN)	Nucleus of the lateral olfactory tract (NLOT)
Superior vestibular nucleus (SUV)	Tuberal nucleus (TU)	
	Tuberomammilliary nucleus, ventral part (TMv)	

* indicates the cell groups whose name is not included in the Allen Mouse Brain Atlas (http://atlas.brain-map.org).

J Comp Neurol. Author manuscript; available in PMC 2017 August 16.